Molecular and spatial landmarks of early mouse skin development

(article starts on next page)

Molecular and spatial landmarks of early mouse skin development

Graphical abstract
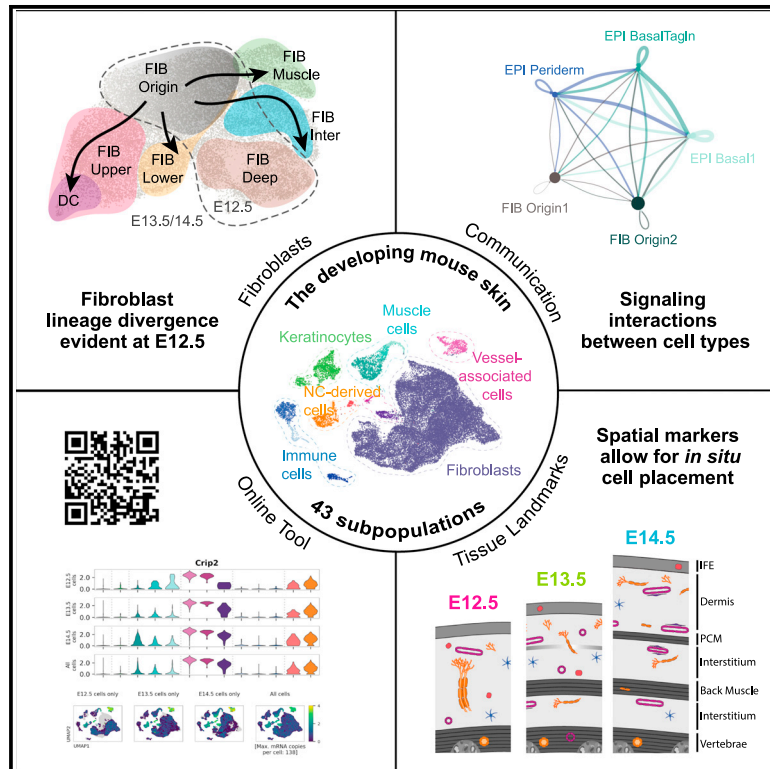
Authors

Tina Jacob, Karl Annusver,
Paulo Czarnewski, ..., Giacomo Donati,
Åsa K. Björklund, Maria Kasper

Correspondence

maria.kasper@ki.se

In brief

Jacob et al. establish a cellular and molecular blueprint of early mouse skin development using single-cell transcriptomics, lineage tracing, and *in situ* multiplex RNA staining. Considering all cell types, they determine molecular and histological key transitions, and cross-cell-type communications, as well as the onset of lineage-diversification during skin development.

Highlights

- Deconstruction of early skin development by scRNA-seq and *in situ* RNA staining

- Fibroblast diversification toward functional lineages starts already at E12.5

- The PCM forms around E13.5 in close association with muscle-supportive fibroblasts

- Unexpected epithelial heterogeneity at E12.5 including a signaling-rich periderm

CellPress

Resource

Molecular and spatial landmarks of early mouse skin development

Tina Jacob,[1,14] Karl Annusver,[1] Paulo Czarnewski,[2,15] Tim Dalessandri,[1,16] Christina Kalk,[1] Chiara Levra Levron,[3] Nil Campamà Sanz,[1] Maria Eleni Kastriti,[4,5] Marja L. Mikkola,[6] Michael Rendl,[7,8,9,10,11] Beate M. Lichtenberger,[12] Giacomo Donati,[3] Åsa K. Björklund,[13] and Maria Kasper[1,17,*]

[1]Department of Cell and Molecular Biology, Karolinska Institutet, 17177 Stockholm, Sweden
[2]Department of Biochemistry and Biophysics, National Bioinformatics Infrastructure Sweden, Science for Life Laboratory, Stockholm University, 17165 Stockholm, Sweden
[3]Department of Life Sciences and Systems Biology, Molecular Biotechnology Center, University of Turin, 10126 Turin, Italy
[4]Department of Physiology and Pharmacology, Karolinska Institutet, 17177 Stockholm, Sweden
[5]Department of Neuroimmunology, Center for Brain Research, Medical University of Vienna, 1090 Vienna, Austria
[6]Cell and Tissue Dynamics Research Program, Institute of Biotechnology, Helsinki Institute of Life Science, University of Helsinki, 00014 Helsinki, Finland
[7]Institute for Regenerative Medicine, Icahn School of Medicine at Mount Sinai, New York, NY 10029, USA
[8]Black Family Stem Cell Institute, Icahn School of Medicine at Mount Sinai, New York, NY 10029, USA
[9]Department of Cell, Developmental and Regenerative Biology, Icahn School of Medicine at Mount Sinai, New York, NY 10029, USA
[10]Department of Dermatology, Icahn School of Medicine at Mount Sinai, New York, NY 10029, USA
[11]Graduate School of Biomedical Sciences, Icahn School of Medicine at Mount Sinai, New York, NY 10029, USA
[12]Skin and Endothelium Research Division, Department of Dermatology, Medical University of Vienna, 1090 Vienna, Austria
[13]Department of Life Science, National Bioinformatics Infrastructure Sweden, Science for Life Laboratory, Chalmers University of Technology, 41296 Göteborg, Sweden
[14]Present address: Schain Research AB, 11151 Stockholm, Sweden
[15]Present address: DeepLife, 75014 Paris, France
[16]Present address: XNK Therapeutics AB, 14157 Huddinge, Sweden
[17]Lead contact
*Correspondence: maria.kasper@ki.se
https://doi.org/10.1016/j.devcel.2023.07.015

SUMMARY

A wealth of specialized cell populations within the skin facilitates its hair-producing, protective, sensory, and thermoregulatory functions. How the vast cell-type diversity and tissue architecture develops is largely unexplored. Here, with single-cell transcriptomics, spatial cell-type assignment, and cell-lineage tracing, we deconstruct early embryonic mouse skin during the key transitions from seemingly uniform developmental precursor states to a multilayered, multilineage epithelium, and complex dermal identity. We identify the spatiotemporal emergence of hair-follicle-inducing, muscle-supportive, and fascia-forming fibroblasts. We also demonstrate the formation of the panniculus carnosus muscle (PCM), sprouting blood vessels without pericyte coverage, and the earliest residence of mast and dendritic immune cells in skin. Finally, we identify an unexpected epithelial heterogeneity within the early single-layered epidermis and a signaling-rich periderm layer. Overall, this cellular and molecular blueprint of early skin development—which can be explored at https://kasperlab.org/tools—establishes histological landmarks and highlights unprecedented dynamic interactions among skin cells.

INTRODUCTION

During skin development, one of the most remarkable changes occurs when the epidermis transforms from a single-layered epithelium to a multilayered and appendage-producing epithelium. Mouse epidermis develops from the surface ectoderm at embryonic day (E) 9.5, starting as a single layer of basal keratinocytes, which is subsequently covered by a transient protective layer of squamous cells called "periderm". Within the following days until birth at approximately E19.5, a fully stratified epidermis is formed, which acts as a reliable barrier keeping pathogens outside and water inside.[1] During these 10 days, also the epidermal appendages form. In dorsal skin, hair follicles develop in three waves, with the first epithelial thickenings—so-called hair placodes—being morphologically visible at E14.5. Hair placodes maintain a tight dialogue with the underlying dermal condensate (DC), a mesenchymal signaling center that stays in close contact with the hair follicle throughout its lifetime.[2–5] The vast majority of studies on embryonic skin to date have focused on the skin's epidermis.[6–8] Nevertheless, important aspects of epidermal development remain unresolved, such as the maturation of the periderm and its signaling potential, basal cell heterogeneity prior to placode formation, and the involvement of mature placode cells in shaping the skin's dermal architecture.
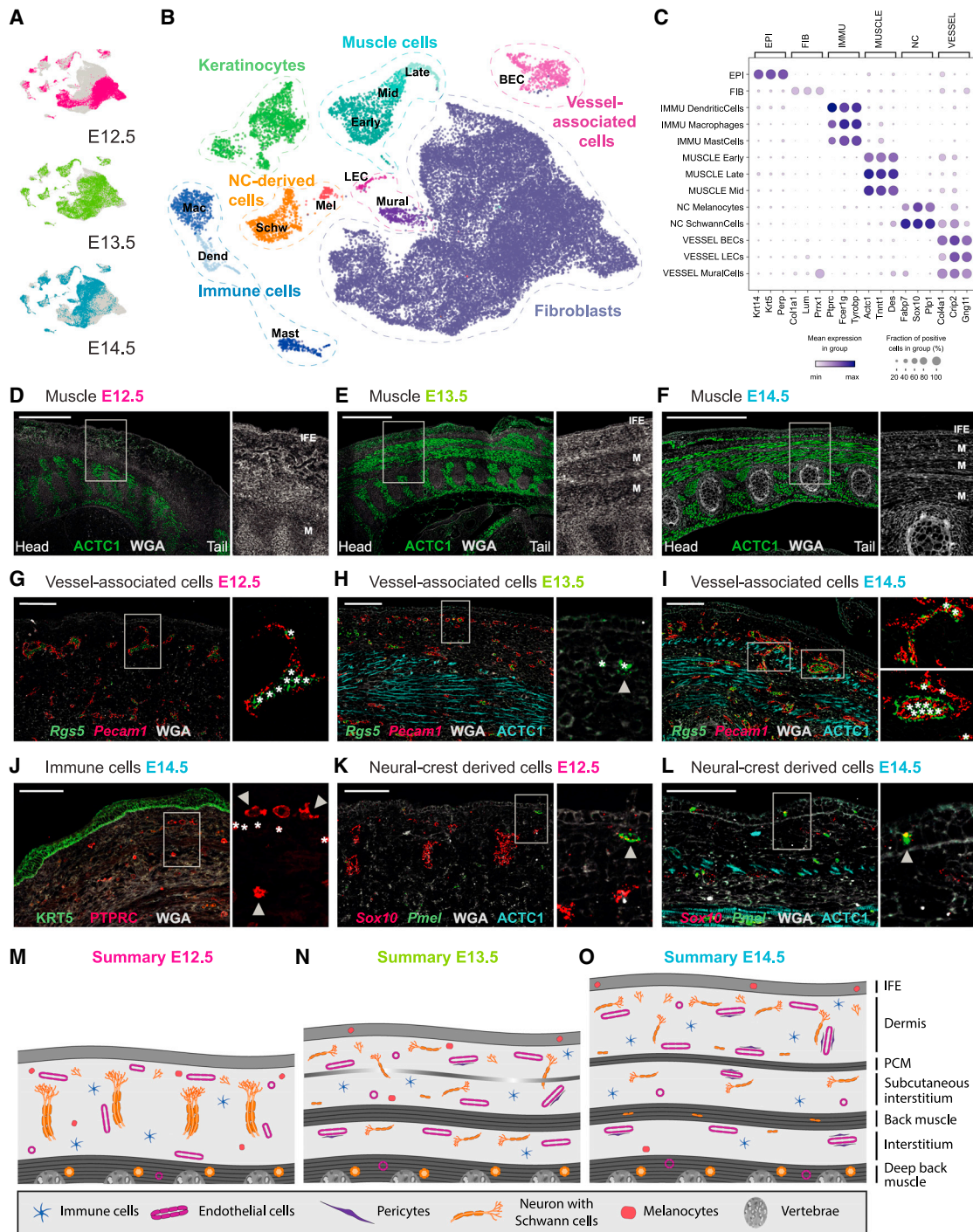
Figure 1. Anatomy of embryonic skin from E12.5, E13.5, and E14.5

(A) UMAP visualization of all cells from the different embryonic ages (n = 11,280 cells at E12.5, 9,964 at E13.5, and 10,950 at E14.5).

(B) UMAP visualization of first-level clustering of all cells (n = 32,194 cells). BEC, blood vascular endothelial cells; LEC, lymphatic endothelial cells; Mel, melanocytes; Schw, Schwann cells; Mac, macrophages; Dend, dendritic cells; Mast, mast cells.

(C) Marker gene expression dot plot for main cell classes.

(D–L) mRNA (italics) and protein (capital letters) staining revealing the major anatomical landmarks of dorsal embryonic skin (sagittal sections). Microscope images originate from larger tile scans (n = 3 mice). Scale bars: 500 μm in (D)–(F) and 100 μm in (G)–(L). * erythrocyte autofluoresence.

(D–F) Muscle layers (ACTC1) with zoom-ins to visualize anatomical layers using membranous counterstain with WGA. M marks developing muscle layers. IFE, interfollicular epidermis.

In the dermis, fibroblasts are the most abundant cell type, yet little is known about their heterogeneity and contributions to early skin development. The few studies that focused on the developing dermis were mostly centered around the molecular and cellular establishment of hair follicles,[9–12] leaving a major gap in knowledge about the non-hair-follicle-related mesenchymal cell types during early skin development. It has been proposed that dermal fibroblasts derive from a single fibroblast lineage that diverges at E16.5 forming the upper (papillary) dermis, including the hair-follicle-associated dermal papillae, dermal sheath and arrector pili muscles, and the lower (reticular) dermis and adipocytes of the hypodermis.[13] Although the existence of fibroblast heterogeneity and potential fate specification prior to the lineage divergence at E16.5 has been proposed,[14] major questions remain. How heterogeneous are fibroblasts during early skin development? When does fibroblast heterogeneity emerge? By which means do early fibroblasts support tissue specification and maturation?

A major challenge to answer any of these questions is the complete lack of histological or molecular tissue landmarks in early developing skin. In adult mouse skin, the only certain landmark to date that defines "skin-associated" cells is the panniculus carnosus muscle (PCM). Only the cells above the PCM (epidermis/dermis), the PCM itself, and a thin layer of connective tissue cells (called fascia) just below the PCM are considered skin-associated. When the PCM is formed has not been reported. At E12.5, the future skin dermis and fascia, as well as non-skin-associated cells, are part of a seemingly homogeneous tissue space spanning from the vertebrae to the epidermis. Similarly, at E13.5 and E14.5, little is known about dermal tissue architecture and cell-type diversity, placing more questions. When does the PCM form? What is the spatiotemporal diversity of all other cell types, such as neural crest (NC)-derived, vessel-associated, or immune cells, during early skin development?

Here, through comprehensive computational analysis of all cell types sampled at E12.5, E13.5, and E14.5, combined with cell-type localization *in situ* and *in vivo* cell-fate mapping, we (1) determined fibroblast heterogeneity and onset of lineage commitment, (2) showed when the PCM forms, (3) resolved the periderm-transcriptome and epidermal cell heterogeneity prior to placode formation, (4) characterized all other major cell types, (5) portrayed the comprehensive interplay between skin cell types, and (6) provided histological landmarks that are essential to place cells in their spatial tissue context.

RESULTS

Single-cell-profiling-assisted generation of histological landmarks in E12.5, E13.5, and E14.5 skin

To unveil the cellular diversity and decisive signaling events driving early skin maturation, we profiled E12.5, E13.5, and E14.5 mouse back skin. We isolated full-thickness dorsal skin and generated single-cell transcriptome (10x v2) libraries of epithelial and stromal cells. To assure true biological replicates, 5 embryos per embryonic time point were processed, sequenced, and quality-controlled individually (Figures S1A and S1B). Moreover, histological analysis of the remaining body of each sequenced embryo as well as intact littermates ensured correct embryonic age (Figure S1C). After quality control, all three time points were analyzed together (Figures S1D–S1F; STAR Methods) to better capture developmental trends and the dynamics of cell populations.

The complete dataset contains 32,194 single-cell transcriptomes with 11,280 cells coming from E12.5, 9,964 cells from E13.5, and 10,950 cells from E14.5 (Figure 1A). Based on cluster-specific gene expression we identified keratinocytes, fibroblasts, immune cells, vessel-associated mural (pericytes and vascular smooth muscle cells [vSMCs]) and endothelial cells, NC-derived melanocytes and Schwann cells, and muscle cells (Figures 1B and 1C; Table S1). Through fluorescent *in situ* hybridization (FISH) for mRNA and immunofluorescence (IF) staining for protein of cell-type-specific marker genes, we mapped all major cell types within E12.5, E13.5, and E14.5 skin tissue (Figures 1D–1L). We also used these cell-type-specific markers together with wheat germ agglutinin (WGA) cell-membrane staining to establish histological landmarks of early skin development, which the commonly used hematoxylin and eosin (H&E) staining cannot resolve (Figures S1G–S1I). Notably, staining for actin alpha cardiac muscle 1 (ACTC1) revealed the stepwise development of multiple muscle layers including the PCM (Figures 1D–1F), PTPRC highlights the exclusively dermal location of immune cells (Figure 1J), *Sox10* shows large nerve trunks growing toward the epidermis at E12.5 and more spread-out nerves at E14.5 (Figures 1K and 1L), and *Rgs5*/*Pecam1* co-staining depicts the dense vascular network (Figures 1G–1I). For this work, these landmarks (summarized in Figures 1M–1O) were instrumental for the mapping and placement of numerous cell populations within the rapidly developing full-thickness skin.

Fibroblast heterogeneity exists long before the reported establishment of papillary and reticular dermis

Our dataset contains in total 25,944 fibroblasts out of 32,194 randomly sampled cells, from 15 individual embryos, allowing for robust identification of 22 fibroblast subpopulations (Figure S2A; Table S2). Overall, fibroblasts isolated from the skin and underlying (non-skin) tissue (see STAR Methods and discussion) separated into seven major cell groups. We named these groups *FIB Origin*, *FIB Deep*, *FIB Upper* & *DC*, *FIB Lower*, *FIB Muscle*, *FIB Inter* and *CHOND* (Figures 2B, 3B, and S2A) based on several criteria such as their appearance in development, their gene-expression profiles, RNA-velocity analysis, and tissue location.

FIB Origin and *FIB Deep*: Notable fibroblast heterogeneity already exists at E12.5

At E12.5, dermis contains the two major fibroblast subsets *FIB Origin* and *FIB Deep*, characterized by expression of unique


(G–I) Endothelial (*Pecam1*) and mural (*Rgs5*) cells. Arrowhead in (H) marks earliest evidence of mural cells at E13.5. Upper zoom-in in (I) shows smaller vessel with discontinuous mural cell lining, while lower zoom-in in (I) shows larger vessel with continuous mural cell lining.

(J) Immune cells (PTPRC) and epidermis (KRT5). Arrowheads highlight immune cells with dendritic phenotype.

(K and L) Melanocytes (*Sox10* + *Pmel*) and Schwann cells (*Sox10*). Arrowhead shows the arrival of melanocytes in the epidermis.

(M–O) Schemes summarizing anatomical landmarks at E12.5, E13.5, and E14.5, respectively.

See also Figure S1.
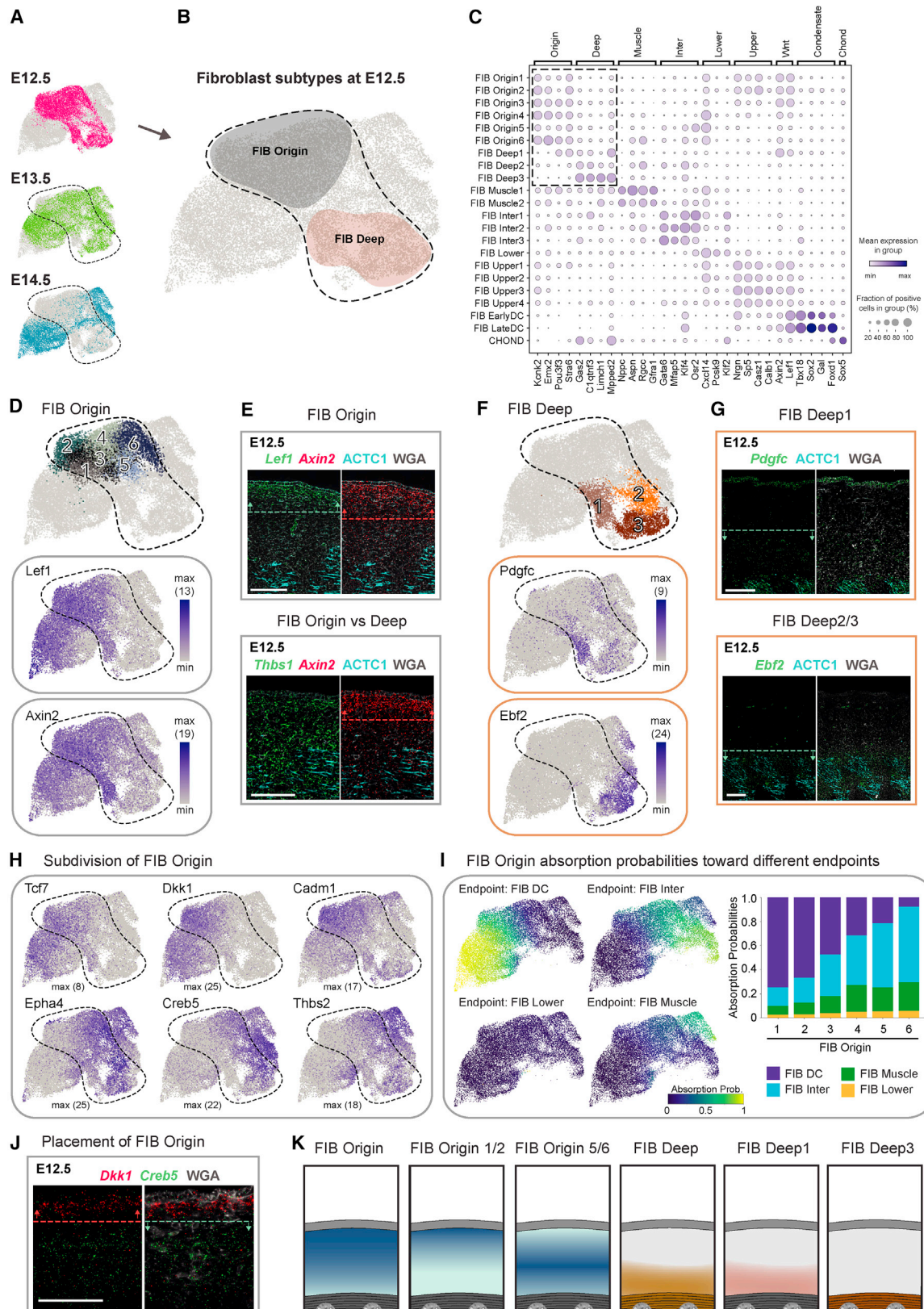
gene sets (Figures 2A–2C and S2C) and different tissue locations (summarized in Figure 2K). The *FIB Origin* cells constitute a Wnt-pathway-activated *Lef1⁺Axin2⁺* fibroblast subset that maps to the upper dermis (Figures 2D and 2E) and expresses remarkably few receptors and ligands (Figure S2E). According to RNA-velocity analysis, which can predict differentiation paths based on the expression of unspliced and spliced mRNA,[15] *FIB Origin* fibroblasts may serve as the source for almost all other fibroblast clusters emerging at E13.5 and E14.5 (Figure S2B). *Lef1* and *Axin2* is also expressed in one of the *FIB Deep* subpopulations at E12.5 (*FIB Deep1*), which is further characterized by co-expression of *Pdgfc* (Figure 2F) and *Hoxb8* (Figure S2F) and maps to the lower half of the subepidermal space (Figure 2G). *FIB Origin* and *FIB Deep1* also share the expression of the myofibroblast markers *Acta2* (also known as α-SMA) and *Tagln* (also known as SM22-α) (Figure S2G). *FIB Deep2* and *FIB Deep3* constitute *Ebf2⁺ Postn⁺* cell populations (Figures 2F and S2H), with *FIB Deep3* additionally expressing *Limch1* (Figure S2F). *FIB Deep2/3* were mapped within the deep back muscle at E12.5 (Figures 2G and S2H).

As the subepidermal/dermal tissue at E12.5 is still a single compartment, which is not yet separated by any muscle layers (see Figures 1M–1O), we considered that not all sampled fibroblasts (and/or their respective lineages) will be part of the skin-associated tissue compartment (i.e., fibroblasts above PCM, within PCM, and in fascia). Based on histological landmarks and tissue placement of *FIB Origin/Deep* subpopulations, *FIB Origin* cells were the most likely source for skin-associated fibroblasts. Thus, we probed whether *FIB Origin* cells are at E12.5 transcriptionally still uniform or already show heterogeneity that may point toward future fibroblast lineages. Unbiased clustering assigned *FIB Origin* cells into 6 subgroups (Figure 2D), which arranged in Uniform Manifold Approximation and Projection (UMAP) dimensionality-reduced space into "left" (*FIB Origin1/2*), "middle" (*FIB Origin3/4*), and "right" (*FIB Origin5/6*) subpopulations. The *FIB Origin1/2* cells are enriched for Wnt-pathway components, such as *Lef1*, *Tcf7*, *Dkk1*, *Sp5*, and the adhesion molecule *Cadm1* (Figures 2C, 2D, and 2H), while the *FIB Origin5/6* cells are marked by, e.g., *Epha4*, *Creb5*, and *Thbs2* (Figure 2H). *FIB Origin3/4* cells are in the UMAP placed between *FIB Origin1/2* and *5/6* cells and express genes of both. Co-staining of markers characteristic for *FIB Origin1/2* (*Dkk1*-enriched) or *FIB Origin5/6* (*Creb5*-enriched) fibroblast subsets revealed a clearly distinct spatial placement, with *FIB Origin1/2* mapping closer to epidermis than *FIB Origin5/6* (Figure 2J). Notably, when overlaying the marker gene expression for *FIB Origin1/2* and *Origin5/6* subsets on the fibroblast

UMAP, the subsets seem to extend into *FIB Upper/DC* and *FIB Inter/Muscle*, respectively (Figures 2H and 3B), suggesting that the subdivision of *FIB Origin* cells may already reflect early commitment toward future fibroblast fates (Figure 3). Indeed, fate simulation of the *FIB Origin* subpopulations confirmed this observation at a global gene-expression level (Figures 2I and S2I; STAR Methods). In summary, we found that skin-associated fibroblast heterogeneity already exists at E12.5 (in *FIB Origin* subsets), representing the earliest reported fibroblast heterogeneity—transcriptionally and spatially—during the development of mouse skin.

CHOND: Embryonic chondrocytes transcriptionally map with skin fibroblasts

Among the 22 fibroblast subsets we identified a small cluster of chondrocytes or their precursors (*CHOND*) that located next to the *FIB Deep* populations in the UMAP (Figures S2A and S2J). Chondrocytes share their developmental origin (paraxial meso-derm-derived somites) with skeletal muscle and the dermis.[16] They express *Pdgfra*, as well as the transcription factors *Sox5* and *Sox6*, which activate the cartilage-promoting factor *Sox9* resulting in the expression of chondrocyte-specific genes such as *Col2a1*, *Col9a3*, *Acan*, and *Matn4*[17–19] (Figure S2K). mRNA staining for the chondrocyte differentiation marker *Mia*[20] showed strong expression in the developing vertebrae (Figures S2L and S2M). Future studies may benefit from the realization that chondrocytes can cluster with fibroblasts.

FIB Upper and *FIB DC*: Acute loss of Wnt inhibitors marks dermal condensate formation

Starting from E13.5, as expected for the time just prior to hair follicle induction, we identified a fibroblast subset (*FIB Upper*) that shows high Wnt-pathway activity (e.g., *Lef1* and *Axin2*) and can mature into the hair-follicle-inductive dermal condensate (DC) (*FIB DC*) (Figures 2D and 3A–3D). This is in line with the current view that Wnt-signaling-activated fibroblasts are a prerequisite for embryonic hair follicle development.[9,10,21–27] *Axin2* mRNA staining revealed that these Wnt-signaling-activated fibroblasts become confined to only a few layers in the uppermost dermis at E13.5 (compare Figures 2E and 3E), a pattern that has been noted before.[21] In line with previous reports,[9,10,12] we also detected that cells exit the cell cycle just prior to DC commitment (upregulation of G0/G1 genes in *FIB DC*, e.g., *Cdkn1a* and *Btg1*) (Figures S2D and S3A) and start expressing *Sox2* when the morphologically recognizable DC is forming (E14.5) (Figures 3D and S2C). These cells also express pre-DC marker *Fst*, early DC markers *Sema6a* and *Fgf10* and, later, DC markers *Dll1* and *Bmp3* (Figure S3B).[9]

Figure 2. Deconstruction of fibroblast heterogeneity at E12.5 (expression and location)

(A) UMAP visualization of fibroblasts from the different embryonic ages (n = 10,008 cells at E12.5, 8,016 at E13.5, and 7,920 at E14.5).

(B) Major fibroblast subtypes at E12.5 highlighted on UMAP.

(C) Marker gene expression dot plot for major fibroblast groups. Highlighted are the clusters mostly present at E12.5.

(D and F) Subclustering of early fibroblast groups (upper). Expression pattern of characteristic marker genes (lower). Number in brackets shows maximum number of RNA copies detected per cell (absolute abundance).

(E, G, and J) mRNA (italics) and protein (capitalized) staining of fibroblast subpopulations. Dashed lines and arrows highlight the region with the highest expression. Microscope images originate from larger tile scans (n = 3 mice). Scale bars, 100 μm.

(H) Marker gene expression of *FIB Origin* subpopulations on UMAP.

(I) Absorption probabilities toward the differentiation end points projected onto UMAP (left) and quantified for each *FIB Origin* subpopulation (right).

(K) Schemes summarizing major fibroblast groups at E12.5 and their locations.

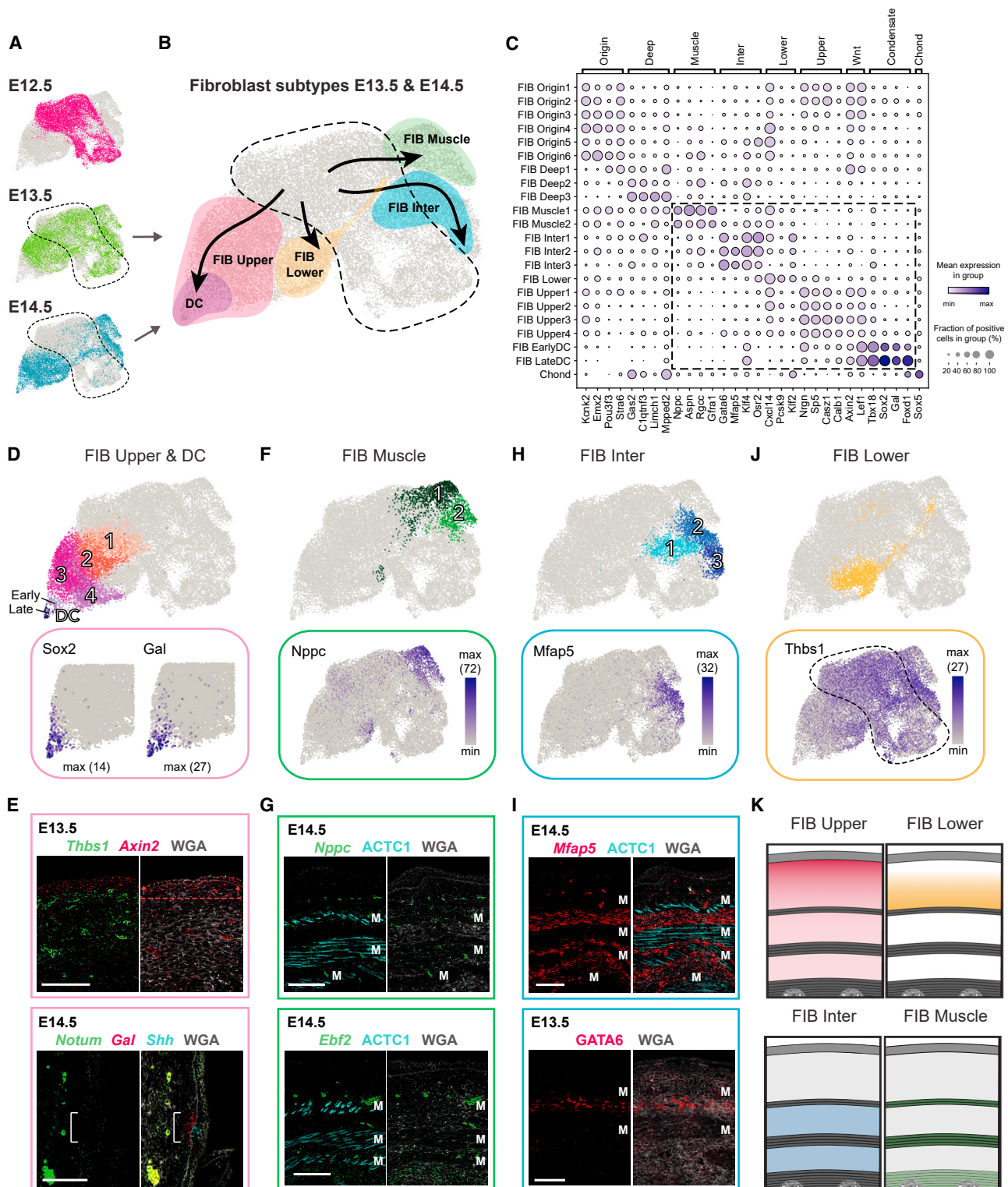See also Figure S2 and Tables S1 and S2.

Figure 3. Deconstruction of fibroblast heterogeneity at E13.5 and E14.5 (expression and location)

(A) UMAP with fibroblasts from different embryonic ages (as shown in Figure 2A).

(B) UMAP showing major fibroblast subtypes at E13.5 and E14.5 together with their differentiation trajectories (velocity trends).

(C) Marker gene expression dot plot for major fibroblast groups. Highlighted are clusters mostly present at E13.5 and E14.5.

(D, F, H, and J) Subclustering of major fibroblast groups (upper). Expression pattern of characteristic marker genes (lower).

(legend continued on next page)

Additionally, our data revealed a most striking and abrupt gene-expression change at both initial and final DC-lineage commitment, each signified by a sharp downregulation of Wnt-pathway inhibitors. At the *FIB Origin* to *FIB Upper* border (E12.5 to E13.5, i.e., initial commitment), we noted acute and permanent downregulation of *Dkk2* (Figure S3A), which is expressed in non-hairy, but absent in hair-bearing skin.[28] Together with our data, this suggests that the absence of *Dkk2* may be a key determinator for fibroblasts becoming competent to enter a DC fate.

As *FIB Upper* cells become more Wnt-pathway activated, they also upregulate *Dkk1* (Figures 2D and 2H). This parallel upregulation continues until DC-fated cells acquire *Sox2* (final commitment), when *Dkk1* expression drops acutely.[9,10] Strikingly, in our data we observe the same switch-like pattern with sharp downregulation at the border between *FIB Upper3/4* and *FIB EarlyDC* also for *Notum* and *Cav1* (Figure S3A), both acting as Wnt-signaling inhibitors.[29,30] The loss of *Notum* expression in mature DC cells was confirmed by co-staining of *Notum* and the DC marker *Gal* in E14.5 skin (Figure 3E). The fact that several prominent Wnt-signaling inhibitors are first upregulated in *FIB Upper* and then abruptly downregulated in *EarlyDC* cells suggests that this is a functional feature of DC formation and/or DC commitment, which remains an exciting route to be explored.

FIB Lower: Dermal fibroblasts without unique marker gene expression

At E13.5 the *FIB Lower* subset emerges. As this cell cluster lacked unique marker genes, we used exclusion criteria that placed this population. At E13.5, *Thbs1* expression becomes confined to the lower dermis as well as to the subcutaneous interstitial layer (Figures 1N and 1O), which starts below the PCM and reaches until the spine[31,32] (Figures 2E, 3E, 3J, 3K, and S3I). In addition to *Thbs1*, the interstitium expresses *Mfap5* (see below), which places *Thbs1*+/*Mfap5*− *FIB Lower* cells to the lower dermis (Figures 3H and 3I).

FIB Muscle: Perimuscular *Nppc*+ fibroblasts possess the ability to support the developing muscle

Also at E13.5, a group of *Nppc*+ fibroblasts (*FIB Muscle*) was first observed (Figures 3B and S2C). This cell population is characterized by expression of *Nppc*, *Rgcc*, and *Gfra1* (Figures 3C and 3F) and is exclusively located within the developing muscle layers (Figure 3G, upper). Subclustering further separated *FIB Muscle* cells into two subgroups, characterized by expression of *Aspn* and *Wnt4* (*FIB Muscle1*), and *Ebf2* and *Igfbp3* (*FIB Muscle2*), respectively (Figures 2F, 3F, and S3C).

As *Wnt4* has been reported to maintain satellite cell quiescence,[33] while *Igfbp3* is known to support myoblast differentiation,[34] it is conceivable that the two *FIB Muscle* subpopulations are involved in balancing activation and quiescence of satellite cells, as has been found in the adult setting.[35] Moreover, *FIB Muscle* cells express high levels of collagen isoforms I, III, IV,

and VI (Figure S3D), which are the primary components of extracellular matrix (ECM) within the skeletal muscles and help to mediate force transmission.[36–46]

FIB Inter: Fibroblasts constituting fascia fibroblasts and a likely source for adipocyte precursors

From E13.5, a distinct group of *Mfap5*+/*Gata6*+ fibroblasts (*FIB Inter*) can be detected (Figures 3B, 3C, and 3H), which mapped to the interstitial layers via ECM component *Mfap5*[47] staining (Figure 3I).

The *FIB Inter1/2* subcluster expressed genes characteristic of the fascia underlying the PCM, such as *Nov, Dpp4,* and *Plac8,*[14,48] as well as the additional fascia-associated genes *Mfap5*, *Wnt2*, *Creb5*, *Col14a1*, and *Tmeff2* (Figures 3H, S3E, and S3F).[48] On the other hand, *FIB Inter3* cells express the key adipogenic transcription factors *Pparg* and *Cebpa* (Figures S3G and S3H; Table S1).[49,50] Given that bundles of fascial fibers are often found mixed with fat to form pressure-tolerant fibro-adipose tissue associated with skin (e.g., soles, palms, or finger tips in humans),[51] we followed up on the intriguing possibility that *FIB Inter* cells might include adipogenic cells. *FIB Inter2* expresses early regulators of adipogenesis *Junb*, *Fos*, *Atf3*, and *Klf4,*[52] while *FIB Inter3* expresses later adipogenesis regulators *Cebpa*[49] and *Pparg*[50] (Figure S3G), suggesting that *FIB Inter2* cells mature to *FIB Inter3* during early adipogenesis. However, these clusters lack the terminal differentiation markers, such as *Fabp4* and *Cd36*[53] (Figure S3G), which appear at approximately E16 and are followed by the characteristic lipid droplets of mature adipocytes appearing at E18.5.[54] In sum, our data suggest that a fibroblast subset may already be fated for the adipose lineage as early as E13.5.

Lineage tracing confirms *FIB Muscle* and *FIB Inter* populations

Because little is known about functionally specialized fibroblasts such as muscle-associated or interstitial fibroblasts, we performed lineage tracing to determine if *FIB Muscle* cells remain muscle-restricted and if *FIB Inter* cells indeed contribute primarily to lower skin layers such as the fascia and adipose tissue as the single-cell RNA sequencing (scRNA-seq) data suggested.

For tracing the *FIB Inter* cells, we identified *Gata6* as one of the most specific cell markers among all skin populations (Figures 4A and 4B). Thus, we used *Gata6-EGFP-CreERT2/R26-tdTomato* (Gata6-Tom) mice and traced *Gata6*+ cells from E13.5 to E15.5 (initial tracing), or to postnatal days P5 and P35 when hair follicles are in active growth (anagen), which is accompanied by an enlarged and mature dermal white adipose tissue (DWAT) compartment (Figure 4C). At E15.5 adipocytes are not yet formed; however, we found Gata6-Tom-traced cells abundantly present in the fascia and the subcutaneous interstitium (Figure 4D). Moreover, tracing to P5 and P35 revealed the persistence of the *FIB Inter* lineage in the fascia from the postnatal stage to early adulthood (Figures 4E and 4F). Unexpectedly

(E, G, and I) mRNA (italics) and protein (capitalized) staining of fibroblast subpopulations. Dashed line with arrows highlights the region of the highest expression. Bracket shows reduced *Notum* expression. M marks developing muscle layers. Microscope images originate from larger tile scans (n = 3 mice). Scale bars, 100 μm.

(K) Schemes summarizing major fibroblast groups at E14.5 and their locations. Similar at E13.5, but PCM is not fully developed yet.

See also Figure S3 and Tables S1 and S2.
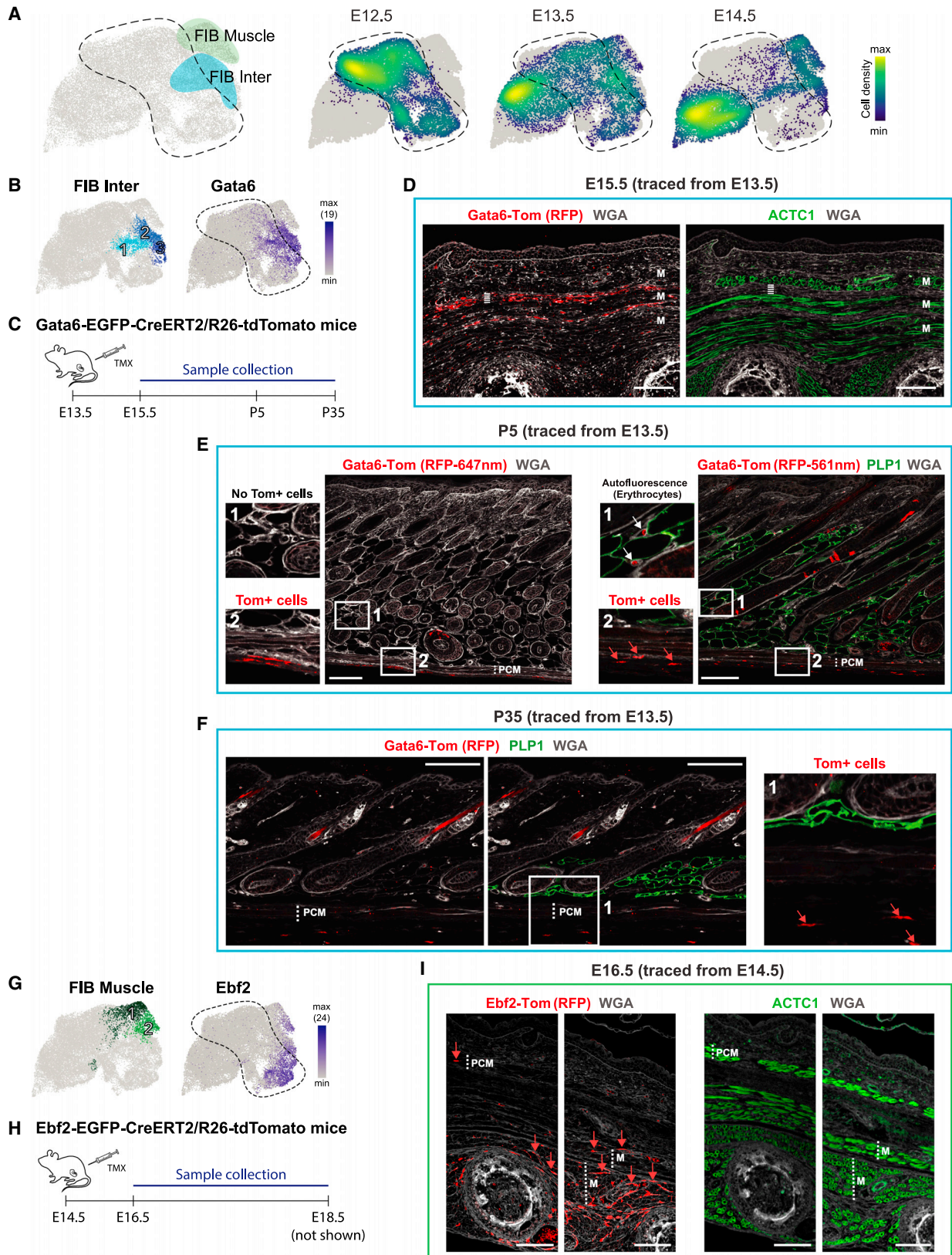
however, we did not detect Gata6-Tom-traced DWAT adipocytes (marked by PLP1 staining) (Figures 4E and 4F), and due to technical limitations, we could not determine if the subcutaneous white adipose tissue (SWAT) was traced. This leaves open two possibilities; *FIB Inter* cells either do not represent adipocyte precursors or *FIB Inter* cells only contribute to SWAT formation and thus DWAT and SWAT originate from independent precursors (see discussion).

To trace the *FIB Muscle* population, *Ebf2* was one of the most suitable markers (at E14.5 expressed in *FIB Muscle2* and *FIB Inter3*) (Figures 4A and 4G). Thus, we utilized *Ebf2-EGFP-CreERT2/R26-tdTomato* (Ebf2-Tom) mice to trace *Ebf2*⁺ cells from E14.5 to E16.5 or E18.5 (Figure 4H). Both 2- and 4-day tracing gave rise to Ebf2-Tom cells within the superficial and deep back muscles and more rarely in the PCM, suggesting that the *FIB Muscle1/2* cell group identified by scRNA-seq indeed constitutes a muscle-associated fibroblast subtype (Figure 4I). As expected from the scRNA-expression pattern (Figures 4A and 4G), Ebf2-Tom tracing also gave rise to some interstitial cells (Figure 4I). Having identified muscle-associated (*FIB Muscle*) and muscle-adjacent (*FIB Inter*) fibroblast populations, we were curious about their potential role in muscle development and its maintenance.

The PCM layer forms *de novo* at E13.5 likely in direct signaling dialogue with *FIB Muscle* and *FIB Inter* cells

Our scRNA-seq data analysis captured the full process of early skeletal myogenesis (Figure 5A). The *MUSCLE Early* population, which encompasses the skeletal muscle stem cells, or *Pax7*⁺ satellite cells,[55,56] constitutes the majority (~70%) of the detected muscle cells (Figure 5A). In comparison, satellite cells in early postnatal life account for 30%–35% and in adulthood 1%–4%.[57] The *MUSCLE Mid* and *MUSCLE Late* populations recapitulate the stepwise expression of myogenic regulatory factors that govern muscle-cell differentiation, with *Myod1* and *Myf5* being early markers for satellite cells that have committed to differentiation and *Myog* and *Myf6* driving terminal differentiation (Figure 5A).[58,59] *MUSCLE Late* cells further express markers of mature muscle-fiber subtypes, e.g., *Tnnc1* for type I and *Tnnc2* for type II fibers (Figure 5A).[60,61] Notably, Syndecans (*Sdc1, Sdc2,* and *Sdc3*), which allow *MUSCLE Early* cells to sense a wide array of signaling that supports muscle formation and maintenance,[62] are downregulated in *MUSCLE Mid* and *MUSCLE Late* cells (Figure S4A). Interestingly, we captured each of the muscle subpopulations (*MUS-*

CLE Early, *Mid*, and *Late*) at all sampled time points (Figure 5A), suggesting that there is no major transcriptional difference between the PCM, superficial, and deep back muscle layers at E12.5, E13.5, and E14.5.

As the PCM is entirely absent at E12.5, we next asked whether the PCM is established through migration of back muscle cells or via *de novo* differentiation within the dermis. To this end, we stained all three developmental time points for *Pax7* mRNA (satellite cells), *Nppc* mRNA (*FIB Muscle*), and ACTC1 protein (the predominant actin isoform in early muscle development[63]) (Figure 5B). At E13.5, we detected the appearance of a noncontinuous PCM layer, with intermingling *Pax7*⁺ satellite cells, *Nppc*⁺ fibroblasts, and some ACTC1⁺ cells. As *Pax7*⁺ cells were entirely absent between muscle layers (i.e., no detectable migrating muscle-precursor cells), we conclude that the PCM may form via direct differentiation at the destined location (Figures 5B and 5C). Moreover, CellChat[64] analysis, which can probe for signaling communication patterns between cell types, suggests strong interactions between muscle cells and fibroblasts (*FIB Muscle/Inter*), strengthening our hypothesis that muscle-surrounding fibroblasts likely support muscle formation and its maintenance (Figures 5D and 5E).
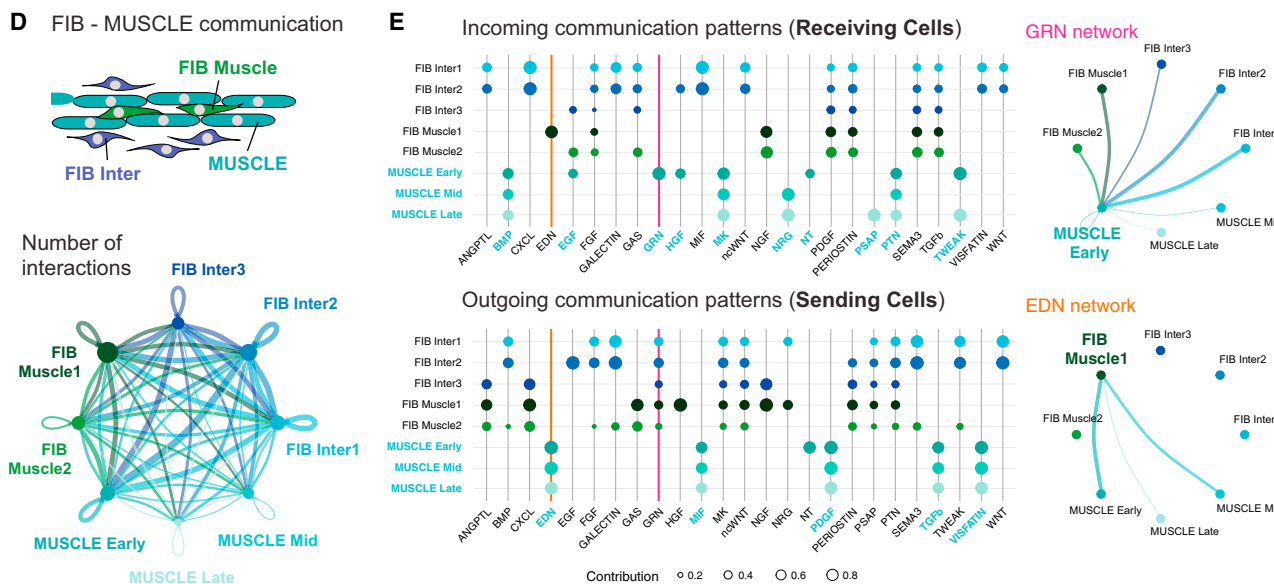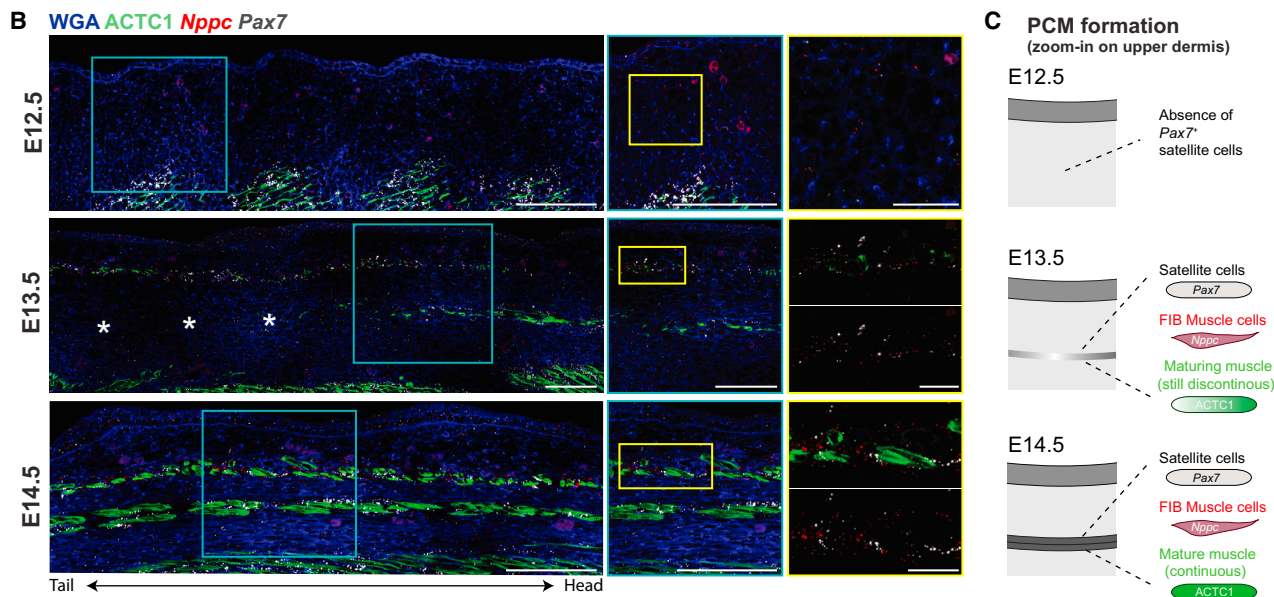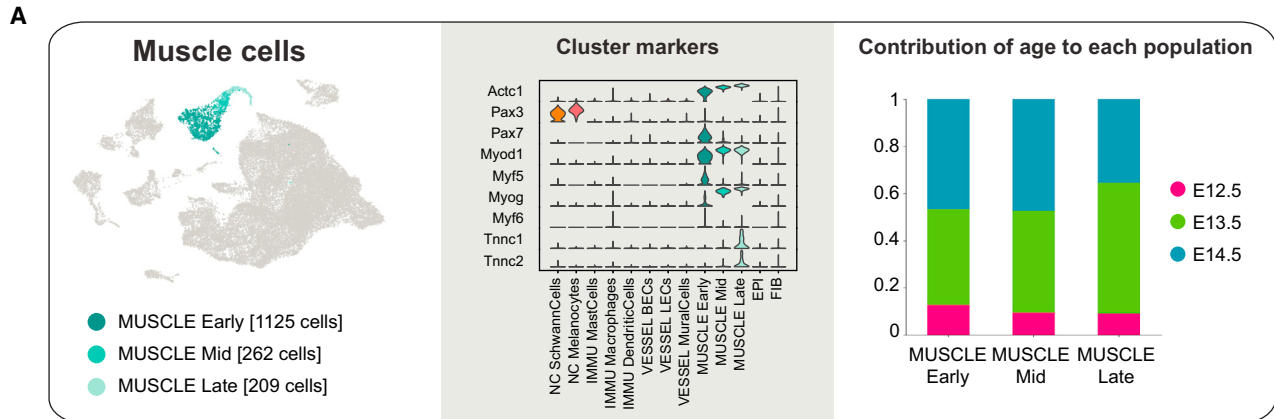
Finally, the PCM and back muscles are, like other skeletal muscles in the body, innervated by motor neurons that connect to the muscle via neuromuscular junctions scattered along the myofibers.[65–67] We indeed find evidence of those neuromuscular junctions in our data (Figure S4B; Table S3), such as *MUSCLE Late* cells expressing *Musk*, which upon binding of ARGN (expressed, e.g., by motor neurons) induces clustering of acetylcholine receptors to form neuromuscular junctions.[68,69] Subunits of those acetylcholine receptors (e.g., *Chrna1*, *Chrna4*, *Chrnd*, and *Chrng*) are expressed in *MUSCLE Mid* and *MUSCLE Late* cells (Figure S4B).

Cellular heterogeneity of vessel-associated, immune, and NC-derived cells in the developing dermis

To reveal the full complexity of dermal cell types, we molecularly characterized the subtypes of vessel-associated cells, immune cells, and neural crest (NC)-derived cells (Figures 6A–6C and S4C–S4F). We then probed for their autocrine and paracrine signaling potentials across cell types using CellChat[64] (Figure 6D) as well as an alternative receptor-ligand (R-L) interaction analysis as used by Joost et al.[70] (Figure S5) with scoring based on a comprehensive hand-curated list of known interactions and annotations (Figure S5; Table S3; STAR Methods).

Figure 4. Tracing the fate of Ebf2⁺ and Gata6⁺ fibroblasts

(A) *FIB Muscle* and *FIB Inter* fibroblasts highlighted on UMAP (left). Density plot showing the distribution of fibroblasts from the different embryonic ages on the UMAP (right).

(B) UMAPs with *FIB Inter* subpopulations (left) and *Gata6* expression (right).

(C) Experimental setup for lineage tracing of *Gata6*⁺ cells.

(D) Initial 2-day tracing pattern of *Gata6*⁺ cells (left) and staining of the developing muscle layers (right). Dashed line marks fascia/SWAT layer on the two consecutive sections. M marks developing muscle layers.

(E and F) Tracing pattern of *Gata6*⁺ cells at postnatal day 5 (P5) (E) or P35 (F) and PLP1 protein staining of lipid droplets. Note the strong erythrocyte autofluorescence within DWAT at 561 nm (E). Dotted lines indicate the PCM.

(G) UMAPs with *FIB Muscle* subpopulations (left) and *Ebf2* expression (right).

(H) Experimental setup for lineage tracing of *Ebf2*⁺ cells.

(I) Two-day tracing pattern of *Ebf2*⁺ cells (left) and staining of the developing muscle layers (right). Dotted lines indicate the PCM and underlying back muscle layers (M) on the two consecutive sections.

(D–F and I) Microscope images originate from larger tile scans (n = 3 mice). Scale bars, 100 μm.

A

Muscle cells

Cluster markers

Contribution of age to each population

- MUSCLE Early [1125 cells]
- MUSCLE Mid [262 cells]
- MUSCLE Late [209 cells]

- E12.5
- E13.5
- E14.5

B

WGA ACTC1 *Nppc* Pax7

E12.5, E13.5, E14.5

Tail ←——————→ Head

C

PCM formation
(zoom-in on upper dermis)

E12.5 — Absence of *Pax7⁺* satellite cells

E13.5 — Satellite cells *Pax7*; FIB Muscle cells *Nppc*; Maturing muscle (still discontinous) ACTC1

E14.5 — Satellite cells *Pax7*; FIB Muscle cells *Nppc*; Mature muscle (continuous) ACTC1

D

FIB - MUSCLE communication

FIB Muscle
FIB Inter
MUSCLE

Number of interactions

FIB Inter3, FIB Inter2, FIB Inter1, FIB Muscle1, FIB Muscle2, MUSCLE Early, MUSCLE Mid, MUSCLE Late

E

Incoming communication patterns (**Receiving Cells**)

GRN network

Outgoing communication patterns (**Sending Cells**)

EDN network

Contribution ○ 0.2 ○ 0.4 ○ 0.6 ○ 0.8

(legend on next page)

Vascular remodeling starts around E13, and sprouting vessels form without pericyte coverage in dorsal skin

Blood vascular endothelial cells (*VESSEL BECs*) and lymphatic endothelial cells (*VESSEL LECs*) were present at all analyzed time points (Figure 6B), which we confirmed in tissue via panendothelial *Pecam1* (CD31) staining (Figures 1G–1I).[71] Cells of the *VESSEL BEC* population express characteristic genes like *Efnb2*, *Ephb4*, *Apln*, and *Aplnr* (Figures 6C and S4C), encoding for proteins that regulate arterial-venous alignment through repulsion (via arterial EFNB2 and venous EPHB4) and attraction (via arterial APLN and venous APLNR).[72,73] *VESSEL LECs* express genes, such as *Lyve1*, *Prox1*, and *Pdpn* (Figure 6C), which are involved in the formation of lymphatic endothelium from venous endothelium as early as E12.5.[74–77]

Ongoing angiogenesis[78] is reflected by *VESSEL BECs* and *VESSEL LECs* from all analyzed time points expressing *Mmp2* and *Dll4* (Figure S4C). Tip cells of sprouting vessels use MMP2 to degrade the vascular basement membrane and DLL4 to prevent neighboring *Notch1*+/*Notch4*+ cells from responding to the key angiogenic factor *Vegfa* (Figure S4C).[79–81] VEGF receptor (VEGFR) expression allows the distinction between *VESSEL BECs* and *VESSEL LECs*, with *Flt1* (VEGFR1) expressed in vascular angiogenesis, *Flt4* (VEGFR3) in lymph angiogenesis, and *Kdr* (VEGFR2) during both processes[82] (Figure 6C). A variety of cells provide typical angiogenic factors (i.e., VEGF family, PDGF family, BMPs, *Tgfb1*, *Pgf*, and ECM components such as *Pcolce*, *Col1a1*, and *Sparc*), and molecules implicated in angiogenesis (Semaphorins, Netrins, Neuropilins, and Slit proteins) (Figures 6D and S5A).[82–88] Notably, keratinocytes (EPI populations) also express high levels of factors such as *Pdgfa*, *Bmp2*, or *Bmp7* (Figures 6D and S5A), fitting the earlier notion that avascular epidermis can stimulate dermal blood supply.[89]

Angiogenesis is followed by vascular remodeling, i.e., the recruitment of mural cells[90,91] encompassing vSMCs and pericytes, which presented as one *Rgs5*+/*Cspg4*+/*Acta2*+ population (Figure 6C).[92,93] Endothelial cells (*VESSEL BECs*) attract the PDGFRB+ EGFR+ mural cells[94] by providing the ligands PDGFB and HBEGF (*Pdgfb* and *Hbegf*) (Figure S4C). Interestingly, we found that mural cells first appear at E13.5, represented by rare *Rgs5*+ cells (Figures 1H and 6B). By E14.5, *Rgs5*+ cells abundantly line small and large vessels (likely representing pericytes and vSMCs, respectively) (Figure 1I). The absence of pericytes at E12.5 is significant because of a long-standing controversy whether sprouting vessels initially form without pericyte coverage[95] or if pericytes are present from the beginning and actively assist vessel sprouting.[96,97] Our data support the first model for embryonic mouse back skin.

Immature skin is already primed with mast cells, dermal dendritic cells, and immature macrophages

Between E12.5 and E14.5, dorsal skin is exclusively populated by myeloid cells, i.e., dermal dendritic cells (*IMMU DendriticCells*), macrophages (*IMMU Macrophages*), and mast cells (MCs) (*IMMU MastCells*) (Figures 1B, 1C, 6A, and 6B). Each of these populations express *Ptprc* (CD45) and are present at all analyzed embryonic time points (Figure 6B and 6C), and exclusively locate to the dermis (Figure 1J).

While dendritic cells and macrophages share the expression of many markers such as *Adgre1* (F4/80), *Itgam*, and *Cx3cr1*,[98,99] they clearly differ in their development and function. Dendritic cell development is critically linked to *Flt3* (Figures 6C and 6D)[100]; they specialize in antigen presenting via MHC-II complexes (e.g., *H2-Aa*, *H2-Ab1*, *H2-Eb1*, *Cd74*, and *Ciita*) (Figures 6C and S4D)[101,102] and express *Ccr2* and *Ccr7*, enabling their migration to the skin-draining lymph nodes to activate T cells (Figure S4D).[103,104] Our dendritic cell population is constituted of classical dendritic cells with the majority being marked by *Itgam* (CD11b) and a smaller fraction expressing *Itgae* (CD103) (Figures 6C and S4D).[98,105,106] To our knowledge, it has not been reported when dendritic cells start seeding the mouse dermis; our data show that they are already present at E12.5 (Figure 6B).

Dermal macrophages are tissue-resident cells that are specialized to scavenge damaged cells or invading bacteria[107] through expressing receptors like *Mertk* and *Stab1*[108] (Figure 6C). Macrophage-like cells seed the dermis as early as E10.5.[109,110] As expected, we detect them at every time point; however, they lack major histocompatibility complex class II (MHC-II) expression and thus mostly represent immature macrophages (Figure S4D). There is a possibility that our macrophage population also contains precursors of Langerhans cells as those can derive from yolk-sac-derived macrophages and share a number of molecular features (*Adgre1*+, *Ptprc*+, *Itgam*+, *Cx3cr1*+, and *Flt3*−) (Figures 6C and S4D).[111,112]

MCs are characterized by expression of *Kit* and serine proteases (e.g., *Cma1*, *Tpsb2*, and *Tpsg1*), which are typical for their secretory granules (Figure 6C).[113] We find MCs already at E12.5 (Figure 6B), displaying the signature of yolk-sac-derived MCs (*Grm6*+, *Cma1*+, *Prss34*+, and *Smpx*+) but still lacking the adult MC signature (*Adrb2*−, *Il1rap*−, *C2*−, and *Lyz1*−) (Figures 6C and S4D). Earlier reports observed sparse dermal MCs only at around E14.5/E15.[114,115]

Leukocyte recruitment to peripheral tissues is directed by chemokines. Via CellChat and R-L analysis we provide a comprehensive expression pattern overview, including the plethora of chemokines involved in leukocyte recruitment (Table S3;

Figure 5. Developing muscle layers in embryonic skin
(A) UMAP (from Figure 1B) with subpopulations of muscle cells (left), violin plot of marker gene expression (center), and contribution of each embryonic time point to subpopulations (right).
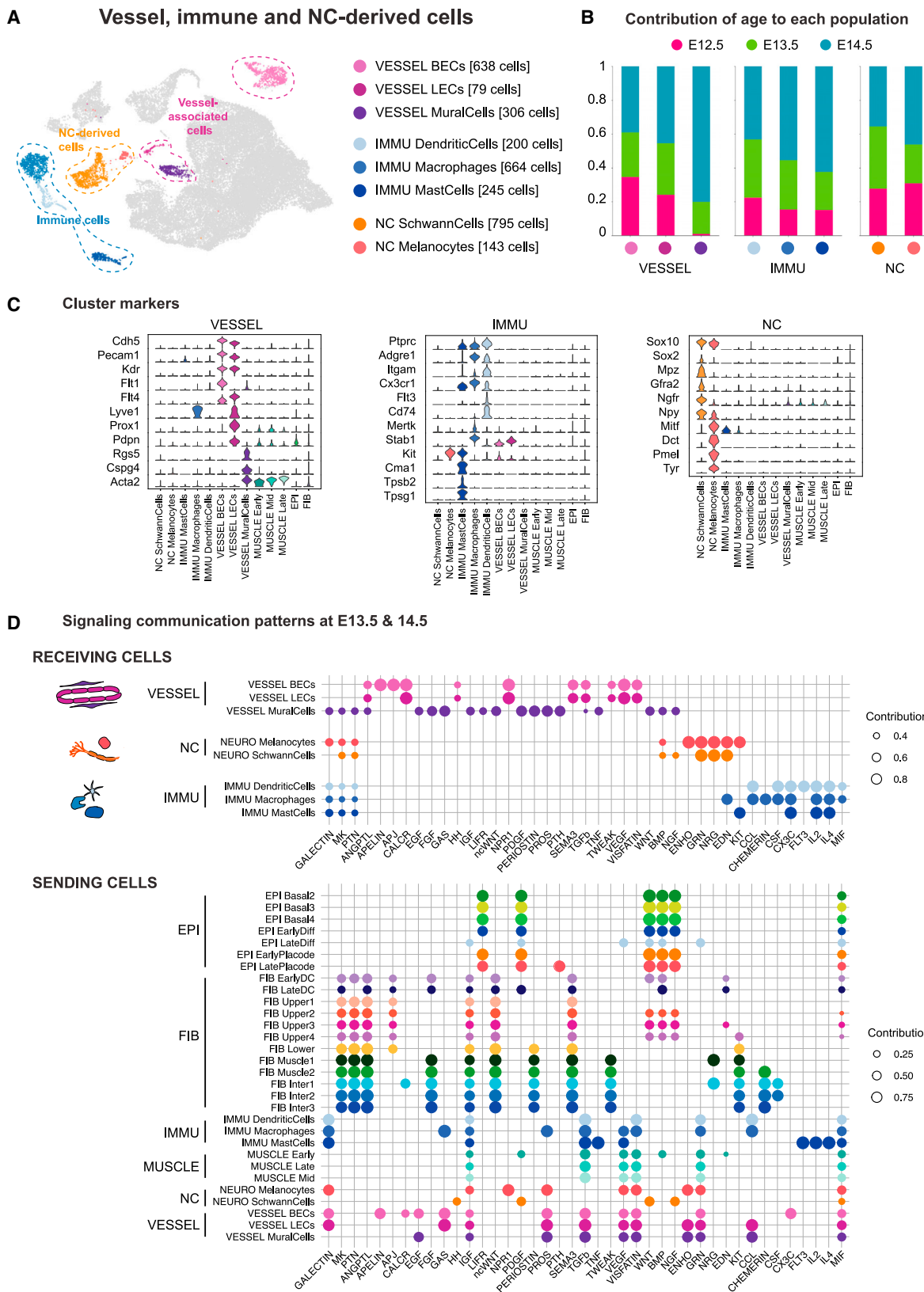(B) mRNA (italics) and protein (capitalized) staining highlighting developing muscle layers. Microscope images originate from larger tile scans (n = 3 mice). Scale bars, 100 μm (panorama, blue zoom-in) and 25 μm (yellow zoom-in). Asterisks indicate a discontinuous upper back muscle layer (dependent on histological cut and distance to dorsal midline).
(C) Scheme of panniculus carnosus muscle (PCM) formation.
(D) Circle plot visualizing the number of interactions between *FIB Inter*, *FIB Muscle*, and *MUSCLE* subpopulations. Edge width is proportional to the number of interactions. Edges colored according to sending cell population.
(E) Dot plot showing outgoing and incoming signaling patterns between *FIB Inter*, *FIB Muscle*, and *MUSCLE* subpopulations (left). Dot size is proportional to the enrichment of signaling pathway in the cell population. Circle plots for selected signaling pathways with significant interactions (right).
See also Figure S4 and Tables S1, S2, and S3.

A   **Vessel, immune and NC-derived cells**

- VESSEL BECs [638 cells]
- VESSEL LECs [79 cells]
- VESSEL MuralCells [306 cells]
- IMMU DendriticCells [200 cells]
- IMMU Macrophages [664 cells]
- IMMU MastCells [245 cells]
- NC SchwannCells [795 cells]
- NC Melanocytes [143 cells]

B   **Contribution of age to each population**

C   **Cluster markers**

D   **Signaling communication patterns at E13.5 & 14.5**

RECEIVING CELLS

SENDING CELLS

(legend on next page)

Figures 6D and S5C). Strikingly, mostly skin-resident immune cells (and partly mural cells) express those chemokines, suggesting their active involvement in skin homing of more immune cells.

Melanocytes and Schwann cells in early embryonic skin

Our dataset contains two NC-derived populations: Schwann cells (*NC SchwannCells*) and melanocytes (*NC Melanocytes*), which are sampled at all three time points and marked, e.g., by *Sox10* expression (Figures 1B, 1C, 6A–6C).[116]

Peripheral neurons have entered embryonic skin at the studied time points,[117,118] which is reflected by the presence of *Sox2*^{+}, *Mpz*[+], *Gfra2*^{+} Schwann cells[119] in our dataset (Figure 6C). Likely due to the distant location of neuronal cell bodies (spinal cord for motor neurons, paravertebral sympathetic ganglia for sympathetic neurons, and dorsal root ganglia for sensory neurons),[120] we did not detect transcriptomes of neuronal cells. Yet, visualizing the nerve-encasing Schwann cells with *Sox10* mRNA and PPARG protein staining[121] revealed thick sensory-nerve trunks traversing the dermis toward the epidermis at E12.5 (Figures 1K and S4E), seemingly splitting up and spreading out as the embryo continues to grow (Figure 1L). At E14.5, nerves are mainly located underneath the epidermis (sensory neurons) and under the PCM (sensory and motor neurons) (Figures 1L and S4E).

Skin innervation is facilitated by neuronal and non-neuronal cells (e.g., fibroblasts and keratinocytes) expressing neurotrophins which are crucial for neuron growth and maintenance (e.g., *Ntf3, Ntf5*, *Bdnf*, and *Ngf*) and a variety of genes that direct the growth cones of developing axons (e.g., Ephrins, Netrins, Slit proteins, and Semaphorins) (Figures 6D, S4F, and S5B).[122–127] In turn, cutaneous nerves also release a variety of neuropeptides, such as *Npy* (neuropeptide Y) (Figure 6C), to increase vascular permeability, support immune-cell recruitment, and induce angiogenesis.[128,129]

The melanocytes in our dataset express the master melanocyte transcription factor *Mitf*, as well as *Dct*, *Pmel*, and *Tyr* (Figure 6C).[130–132] Melanocytes migrate through the dermis around E12.5 and enter the epidermis around E13.5,[133,134] supporting our finding of gradual migration of *Sox10*^{+}/*Pmel*^{+} cells from the dermis at E12.5 (Figure 1K) to spread throughout the epidermis by E14.5 (Figure 1L), where they will eventually persist only in adult hair follicles.[135] This melanocyte recruitment is supported by fibroblasts and epidermal keratinocytes, expressing factors like *Edn1*, *Edn3*, *Kitl*, and *a* (agouti) (Figures 6D, S4F, and S5B).[130,136]

Basal epidermal keratinocyte heterogeneity starts already at E12.5

At E12.5, the epidermis consists of keratinocytes that form a morphologically uniform basal layer that is covered by the peri-

derm. Surprisingly, the E12.5 basal cells separated into two transcriptionally distinct populations, which we termed *EPI BasalTagln* and *EPI Basal1* (Figures 7A–7C, S6A and S6C). *EPI Basal1* cells have no unique molecular signature within keratinocytes. Their characteristic genes are shared with either *EPI BasalTagln* from E12.5 skin (e.g., *Olfm1*, *Bfsp2*, *Acvr2a,* and *Podxl*), with *EPI Basal2–4* populations from E13.5 and E14.5 skin (e.g., *Lmo1*, *Dcn*, and *Ifitm3*) or with all basal populations (e.g., *Krt5, Krt14, Krt15, Sostdc1,* and *Vcan*) (Figure S6B). In contrast, *EPI BasalTagln* cells express a unique set of genes including *C1qtnf3*, *Hapln1*, *Tagln*, *Cldn11*, *Amtn*, *Myl9*, *Bambi*, and many more (Figures 7D and 7E; Table S1). Remarkably, *EPI BasalTagln* cells also express smooth muscle genes such as *Tagln* (SM22a) and *Myl9* (Figure 7D), which is highly unexpected for epithelial cells under physiological conditions. Compared with all basal cell clusters, *EPI BasalTagln* cells express a high number of receptors and ligands, including higher levels of *Wnt3a, Wnt4*, and *Wnt6,* and exclusive *Wnt2* expression (Figures 7D and S6E; Table S1), which were commonly believed to be uniformly expressed throughout embryonic epidermis.[22,137] Notably, CellChat analysis predicts that both basal populations are equally engaged in auto- and paracrine cell-type interactions (Figures S6F–S6J), leaving the role of these two transcriptionally distinct populations entirely open. Based on gene expression and their position in dimensionality-reduced space it seems more likely that *EPI Basal1* cells are the precursors for the general interfollicular epidermis (IFE) at E13.5 and E14.5 (Figures 7A and S6A). In comparison with E12.5, basal IFE at E13.5 and E14.5 appears rather uniform transcriptionally. The *EPI Basal2-4* populations do not display unique marker genes and overall only show minor expression differences (Figure S6B; Table S1) and fewer specific receptors or ligands (Figure S6E).

The periderm matures and exhibits a signaling-rich molecular signature

Periderm is a curious specialization of embryonic epidermis. It is a layer composed of squamous cells that cover the epidermis, and its presence is crucial for preventing pathological epithelial adhesions within the embryo.[138] Periderm cells start covering dorsal epidermis around E10 (delaminating from the basement membrane to cover basal keratinocytes) and are shed around E17/18 when the cornified layer forms.[139–141] Although the existence of this layer has long been known, its molecular characterization has remained incomplete even in the era of scRNA-seq (see discussion). In our data, we robustly identified periderm cells (*EPI Periderm*) at all three time points (Figures 7A, 7B, S6A and S6C), likely due to the large cell proportion relative to all epithelial cells at E12.5. We identified a number of periderm markers including well-known (e.g., *Cldn6/23*, *Krt6/8/17/18/19*, *Grhl3*, and *Sfn*) and additional ones (e.g., *Myh14*, *Paqr6*, *Tgfb2*, and *Sox9*), of which *Cldn6, Krt17, Grhl3, Sfn*,[138,141–144] and *Sox9* are not uniquely

---

Figure 6. Vessel, immune, and neural crest (NC)-derived subtypes and signaling interactions for their respective establishment in embryonic skin

(A) UMAP (from Figure 1B) with subpopulations of vessel-associated cells, immune cells, and NC-derived cells.

(B) Contribution of each embryonic time point to subpopulations.

(C) Violin plots of marker gene expression.

(D) Dot plot showing the enrichment of signaling pathways received by vessel-associated, immune, and/or NC-derived cells.

See also Figures S4 and S5 and Tables S1, S2, and S3.

A Keratinocyte subtypes (UMAP)

B E12.5, E13.5, E14.5

C E12.5, E13.5, E14.5

BasalTagln, a major basal population at E12.5

D / E *Hapln1* WGA (E12.5)

Periderm at E12.5, 13.5 and 14.5

F / G SOX9, *Sox9* WGA, SOX9 WGA, *Krt8* WGA (E14.5, E12.5)

IFE differentiation at E13.5 and 14.5

H / I Clustering Age Krt15 Krt14 Krt10 Krtdap Krt5 / J *Krt5 Krtdap* WGA (E14.5)

K Potential early drivers of stratification

Hair follicle placode formation at E13.5 and 14.5

L / M *Ltb Shh Ptch1* WGA (E13.5) / N *Dkk4 Shh Gal* WGA (E13.5) / O *Ltb Shh Ptch1* WGA (E14.5) / P *Dkk4 Shh Gal* WGA (E14.5)

(legend on next page)

expressed in *EPI Periderm* among *EPI* populations (Figure 7F; Table S1). Interestingly, periderm cells are the unique receivers of GRN signaling and constitute a source for TGFb signaling which can be received by epidermis-near E12.5 fibroblasts (Figure S6I). Interestingly, *Sox9* and *Krt8*, known for their roles in hair follicle formation and as a marker of the immature epidermis, respectively, show their highest mRNA expression in periderm cells (Figures 7F and 7G). Additionally, we observed a basal (placode periphery) and suprabasal (IFE-associated) *Sox9* expression pattern as reported recently (Figure 7G).[145]

Cells within the periderm still divide (Figure S6D).[138] In addition, we found that the periderm undergoes a molecular maturation characterized by increased expression of known IFE differentiation markers (e.g., *Krtdap*, *Lgals3*, and *Dkkl1*), and multiple genes that have not been linked to IFE differentiation, such as *Foxq1*, *Krt4*, *Lingo2*, *Mal*, *Pllp*, *Prss27*, and *Tchh* (Figure S7A). Surprisingly, within keratinocyte clusters, periderm cells express the highest numbers of receptors and ligands (Figure S6E), including those facilitating e.g., Ephrin signaling, Notch signaling, and Tgfb signaling (Table S1).

Deconstructing early epidermal stratification

Differentiating keratinocytes separate into an early differentiating group (*EPI EarlyDiff*) marked by co-expression of basal (e.g., *Krt15*, *Krt14*, *Vcan*, *Lmo1*, and *Sostdc1*) as well as suprabasal genes (e.g., *Krt10*, *Krtdap*, and *Aqp3*), and a more mature differentiating population (*EPI LateDiff*), which has gradually lost basal-gene expression and further increased differentiation-related gene expression (e.g., *Slc7a11*, *Tgm3*, and *Serpinb3a*) (Figures 7H and 7I). In line with previous reports of differentiation initiating at E13,[146,147] we detect the first differentiating *EPI EarlyDiff* cells at E13.5, and *EPI LateDiff* at E14.5 (Figure S6C). *In situ* staining further revealed that some rare *Krt5*+ basal layer cells already start upregulating *Krtdap* even though they have not delaminated yet (Figure 7J).[148] Interestingly, although Keratins 5 and 14 usually co-polymerize, in suprabasal cells of embryonic skin *Krt14* is strictly downregulated while *Krt5* expression persists, and in the hair placode it is *vice versa* (Figures 7I, S7B, and S7C).

As the early signals that make a basal cell commit to differentiation are not fully resolved in embryonic skin, we utilized our da-taset to identify potential drivers. After performing rigorous cell-cycle corrections—this was the dominating factor in initial velocity analysis—we obtained a clear differentiation pseudo-time trajectory from *EPI Basal2/4* cells toward *EPI EarlyDiff/Late-Diff* cells (Figure S7D) and early pseudotime-dependent genes (Figure 7K). *Notch1*, a known commitment switch in epidermal differentiation[149,150]; *Cdh1* (E-cadherin), which is responsible for altered adhesion properties that allow keratinocytes to differentiate[151]; and *Grhl3*, which facilitates epidermal stem cell differentiation[152] were among the top hits on our list, suggesting that our gene list likely contains additional (but not yet functionally tested) differentiation drivers. The upregulation of these genes appears to be transient or at least most pronounced in early differentiation supporting a potential switch-like function (Figures 7K and S7D).

Hair placodes engage in the establishment of blood vessels, nerves, and immune environment

The epithelial counterpart to the DC, which is necessary for hair follicle formation, is the hair follicle placode. While placodes became morphologically first visible at E14.5 (Figures S1H and S1I), cells with transcriptional signs of a placode fate were already detected at E13.5 (*EPI EarlyPlacode* and *EPI LatePlacode*) (Figures 7A–7C and S6C). *EPI EarlyPlacode* cells express the placode markers *Fgf20* and *Dkk4*, but still lack more mature markers like *Shh* and *Lhx2*[153,154] (Figure 7L). *In situ*, they can be captured at E13.5 by *Dkk4* and *Ltb* staining (Figures 7M and 7N). *Shh* was detected centrally within the more mature placode,[145] while other markers such as *Ltb* showed a slightly broader expression pattern (Figures 7O, 7P, and S7E). Interestingly, placode cells downregulated only a handful of genes (e.g., *Gas1*, *Krt5*, and *Hspb1*) but upregulated numerous genes, suggesting that placode commitment is determined by the gain, rather than the loss, of expression (Figure 7L). While reporter mice and *in situ* mRNA staining have long revealed that placode patterning begins prior to E14.5,[27,155–157] previous scRNA-seq studies of embryonic skin did not reveal those E13.5 cells with early placode markers likely due to the choice of a different analysis strategy.[10]

Finally, our R-L analysis (Figures 6D and S5A–S5C) suggests that the nascent placode and DC cells immediately engage in

---

Figure 7. Epidermal development from a single basal layer toward a hair follicle (HF)-inducing and stratified epithelium

(A and B) UMAP visualization of all keratinocyte subclusters (A) and their embryonic ages (B) (n = 360 cells at E12.5, 347 at E13.5, and 877 at E14.5).

(C) Scheme summarizing epidermis development in the analyzed time window, with cells colored according to the cluster colors in (A).

(D) Violin plot of *EPI BasalTagln* marker gene expression.

(E) *Hapln1* mRNA staining revealing the expression in basal IFE (arrowheads).

(F) Violin plot of periderm marker gene expression.

(G) SOX9 protein staining (left); expression in periderm (filled arrowheads) and hair placode cells (asterisks). *Sox9* mRNA staining (upper right); expression in cells within and outside of hair placode (asterisk and empty arrowheads, respectively). *Krt8* mRNA staining; expression in periderm cells (filled arrowheads).

(H) Violin plot of differentiation marker gene expression.

(I) UMAPs of differentiating keratinocytes (*EPI EarlyDiff* and *EPI LateDiff* from A) colored according to subclustering and embryonic age (left two panels) or expression of basal and suprabasal marker genes (right).

(J) *Krt5* and *Krtdap* mRNA staining reveals a representative basal cell with a differentiation signature (arrowhead).

(K) Heatmap of potential early drivers of stratification along the pseudotime from *EPI Basal1-4* to *EPI EarlyDiff* and *EPI LateDiff* cells from E14.5 (see Figure S6I). *Krtdap*, *Krt10*, and *Slc7a11* are plotted for comparison.

(L) Violin plot of hair placode marker gene expression.

(M–P) *Ltb*, *Shh*, and *Ptch1* (M and O) or *Dkk4*, *Shh*, and *Gal* (N and P) mRNA staining at E13.5 (M and N) and E14.5 (O and P), showing early placode cells (M and N; arrowheads) and mature hair placodes (marked by *Ltb*, *Shh*, and *Dkk4*) as well as dermal condensates (marked by *Ptch1* and *Gal*).

(E, G, J, and M–P) Images originate from larger tile scans (n = 3 mice). Scale bars, 50 μm.

See also Figures S6 and S7 and Tables S1 and S2.

reciprocal interactions with crucial cell types for blood supply (*Bmp2, Bmp7,* and *Mfge8*), innervation (*Bdnf, Nrtn, Ntf3,* and *Edn3*), and immune support (*Tnf* and *Ltb*)[158–161] (Figure S7F).

DISCUSSION

The most insightful transcriptional investigations of early embryonic skin to date have relied on known markers and averaged transcriptomes (bulk RNA-seq of FACS-sorted populations)[162] or focused their scRNA-seq analysis on specific cell types/processes such as the molecular origin of IFE cells,[163] the cellular origin of hair follicle stem cells,[145] or placode- or DC-fate specification.[9,10,164]

The work at hand leveraged scRNA-seq analysis of randomly sampled cells at E12.5, E13.5, and E14.5 to paint a holistic picture of early skin development. Through comprehensive computational analysis of all sampled cells, cell-type localization *in situ*, and *in vivo* cell-fate mapping, we answered major outstanding questions in mouse skin development and made unexpected discoveries. When and where does skin begin? How heterogeneous are fibroblasts prior to DC formation? Is the periderm merely a signaling-inert protective layer to be shed at birth?

When and where does skin begin: Setting detailed anatomical and molecular landmarks

Until now, E12.5 dermis and underlying non-skin-associated cells were perceived as a seemingly homogeneous tissue covering the area between the vertebrae and epidermis. Similarly, little was known about dermal tissue architecture and cell-type diversity at E13.5 and E14.5. Thus, it was critical to sample, without bias, the skin and the underlying tissue at full thickness from E12.5 to E14.5 (see STAR Methods) to establish anatomical and molecular tissue landmarks of the skin and the underlying tissue.

One of the most important landmarks to define cell populations as skin-associated in mouse is the PCM. While it is well-known that the PCM originates from the E9.5 *Pax7*+ dermomyotome,[165–167] its histological emergence had not been documented. By combining RNA and protein staining for early and mature muscle cells and the muscle-associated fibroblasts defined in this study, we revealed the emergence of the PCM (Figures 5B and 5C). The PCM and other developing muscle layers were used as landmarks to place our scRNA-seq subpopulations. Altogether, this extensive back-mapping effort generated a detailed molecular tissue guide that complements previous findings and accelerates the interpretation of future findings.

Fibroblast heterogeneity and the emergence of papillary and reticular dermis

It has been the accepted view that dermal fibroblasts constitute a "uniform cell type" until E16.5, when they finally commit to two different lineages generating upper papillary and lower reticular dermis.[13] Our data reveal that molecular and functional diversity of fibroblasts is already established at E13.5, with further specification at E14.5, when the DC forms (Figure 3). We also find clear transcriptional heterogeneity in E12.5 dermis (Figure 2), pointing at a fate bias toward distinct fibroblast subtypes. To what degree these early lineages remain plastic or are already fate-restricted under homeostatic conditions remains to be determined.

Driskell et al. also established a molecular distinction of fibroblasts into papillary dermis (DPP4+/DLK1−/LY6A−), reticular dermis (DPP4−/DLK1+/LY6A+), and hypodermis (DPP4−/DLK1−/LY6A+) starting from late embryogenesis. They detected DLK1 protein expression throughout the dermis until E16.5, while lineage-specific DPP4 (CD26) and LY6A emerged around E16.5.[13] We observed *Dlk1* expression throughout the dermis (see online tool: https://kasperlab.org/embryonicskin) and detected cells with a *Ly6a*+/*Dpp4*+ double signature in the *FIB Inter* population starting from E13.5 (Figure S3E), raising the question if there is a relationship between our *Dpp4*+/*Ly6a*+ *FIB Inter* cells and the papillary and reticular dermis. As we observe *FIB Inter* cells at a time when *FIB Upper* and *FIB Lower* cells (the tentative precursors of papillary and reticular dermis; *Dpp4*−/*Ly6a*+) have already been established, it is likely that *FIB Upper* and *FIB Lower* cells develop in parallel to *FIB Inter* cells.

Remarkably, the early existence of spatially defined fibroblast layers resembles the dermal structure of healing wounds. Similar to the developing skin, where spatial layering of fibroblasts is one of the earliest morphogenic events and intriguingly precedes morphologically definable development events, such as hair follicle morphogenesis and dermal adipose morphogenesis; also, the healing wound shows spatial segregation of transcriptionally distinct fibroblasts even days before *de novo* hair follicles are established in the regenerating epidermis.[13,168–172]

Revisiting early progenitors of dermal and subcutaneous white adipose tissue

In 2013, Wojciechowicz et al. postulated a possible presence of pre-adipocytes already at E14.5, which our scRNA-seq data clearly support.[54] Cells within the *FIB Inter2/3* populations increasingly express typical adipogenic genes (e.g., *Pparg* and *Cebpa*), suggesting the presence of adipocyte precursors (Figures 3H and S3G). *In situ* staining for *Pparg* mRNA and protein in E14.5 skin (Figure S3H) revealed *Pparg*+ cells within the subcutaneous interstitium or just above the PCM, future sites for the SWAT and the DWAT, respectively.[173] Notably, our *FIB Inter2/3* cells match recent descriptions for adipose mesenchymal progenitors (*Dpp4*+/*Anxa3*+/*Wnt2*+) in human as well as murine skin,[32] and for *Dpp4*+/*Ly6a*+/*Cd55*+ adipose stem cells[53] (Figures S3E and S3F).

Given this concurrence with the literature, it was surprising that we did not observe any Gata6-Tom-traced adipocytes. As we started tracing at E13.5, when the SWAT and DWAT are not yet separated by the PCM, we in principle should have found Tom-traced cells in both compartments, or at least in one of them. However, we did not find traced DWAT cells and due to technical limitations, SWAT was lost when harvesting postnatal skin. This leaves us with three open possibilities: (1) *FIB Inter* cells do not represent adipocyte precursors at all, which is unlikely based on their expression of adipogenic genes; (2) tracing at E13.5 is not efficient enough to label the adipose progenitors; or (3) DWAT and SWAT originate from independent precursors, where *FIB Inter* cells only contribute to SWAT formation. This is supported by their locations on opposite sides of the developing PCM and by the current view that DWAT is morphologically and developmentally distinct from SWAT.[54,173] As the latter view is derived from experiments performed from E14.5 onward, the earliest determination of a fibroblast subset toward generating

DWAT and/or SWAT tissue remains an interesting route to be explored.

Unexpected heterogeneity in E12.5 epidermis and a surprisingly signaling-rich periderm

We identify significant heterogeneity in E12.5 epidermis, which to date had been considered a uniform epithelial sheet. The identified distinct *EPI BasalTagln* population could have a possible role in transient signaling during skin development (e.g., to activate the upper dermis via Wnts),[174–176] or it could be a source for the periderm as indicated by a shared transcriptional signature (Table S1), but its exact function remains elusive. In comparison, IFE basal cells at E13.5 and E14.5 were transcriptionally very similar. Subclustering of *Basal2-4* likely represents cell-cycle influences, rather than populations with distinct behaviors or functions. Interestingly however, we observed rare differentiating basal cells (Figure 7J), reminiscent of delaminating *Krt10*^{+} cells in adult mouse skin.[148] Thus, it is tempting to speculate that epidermal stratification in embryonic skin may be fueled by two coexisting basal cell behaviors: (1) delamination triggered by basal cell crowding as the predominant mechanism[147,151] and (2) delamination through gradual differentiation, which is the main mechanism in postnatal and adult skin.[148,152]

The existence of periderm cells in embryonic skin has long been known.[139] However, due to lower periderm cell numbers in previous scRNA-seq studies,[10,11,163] these cells were likely hidden within other keratinocyte clusters, such as differentiated IFE cells, due to periderm cells expressing typical IFE differentiation genes like *Grhl3* and *Zfp750* (Figures 7F and 7H). Notably, transcriptional characterization of the periderm revealed that it is highly signaling-prone (Figure S6E), which raises the possibility of previously unrecognized "non-canonical" periderm functions in embryonic skin development.

Limitations of the study

In this work we present all identified cell populations (cell types, subtypes, and states) among all randomly sampled cells from embryonic skin. At first sight an overwhelming amount of information, the analysis and presentation of all cell populations within one study advances our understanding from studying individual cell types (in isolation) to their communal functions at the tissue level—revealing insights that cell-type-focused studies would not be able to uncover. However, given the vast amount of data, we had to focus our analysis on major outstanding questions such as the emergence of fibroblast and keratinocyte heterogeneity or the development of the PCM. Therefore, some cell types lack in-depth analysis and the current data interpretations may represent purely data-driven suggestions, rather than final conclusions, and require further exploration in future studies.

STAR★METHODS

Detailed methods are provided in the online version of this paper and include the following:

- KEY RESOURCES TABLE
- RESOURCE AVAILABILITY
  ○ Lead contact

- ○ Materials availability
  ○ Data and code availability
- EXPERIMENTAL MODEL AND STUDY PARTICIPANT DETAILS
  ○ Mouse work
- METHOD DETAILS
  ○ Replicates
  ○ Tissue embedding
  ○ Fluorescent *in situ* hybridization (FISH)
  ○ Immunofluorescence (IF)
  ○ Imaging and image analysis
  ○ Cell isolation
  ○ Library preparation, sequencing and processing of sequencing data
- QUANTIFICATION AND STATISTICAL ANALYSIS
  ○ Data analysis

AUTHOR CONTRIBUTIONS

M.K. and T.J. formulated the research question and designed the study. T.J. performed all single-cell sequencing experiments including animal work and cell isolation. T.J. and T.D. sampled tissue for validation experiments. T.J. performed the majority of the bioinformatic data analysis. K.A., P.C., C.K., and Å.K.B. contributed to bioinformatic data analysis. T.J. planned and set up validation staining (protein-IF and RNA-FISH). T.J., K.A., and N.C.S. performed and imaged validation staining. T.J. and C.L.L. performed lineage tracings in mice, and K.A. and M.K. analyzed the tracing patterns. T.J., K.A. and N.C.S. performed image processing. B.M.L., M.R., M.L.M., T.D., and M.E.K. helped to interpret the results. G.D. provided Gata6-tracing mice. M.K. and T.J. wrote the manuscript with input from all authors.

REFERENCES

1. De Falco, M., Pisano, M.M., and De Luca, A. (2014). Embryology and anatomy of the skin. In Current Clinical Pathology. Skin Cancer, A. Baldi, ed. (Springer Science+Business Media), pp. 1–15. https://doi.org/10.1007/978-1-4614-7357-2.

2. Biggs, L.C., and Mikkola, M.L. (2014). Early inductive events in ectodermal appendage morphogenesis. Semin. Cell Dev. Biol. 25–26, 11–21. https://doi.org/10.1016/j.semcdb.2014.01.007.

3. Sennett, R., and Rendl, M. (2012). Mesenchymal-epithelial interactions during hair follicle morphogenesis and cycling. Semin. Cell Dev. Biol. 23, 917–927. https://doi.org/10.1016/j.semcdb.2012.08.011.

4. Saxena, N., Mok, K.W., and Rendl, M. (2019). An updated classification of hair follicle morphogenesis. Exp. Dermatol. 28, 332–344. https://doi.org/10.1111/exd.13913.

5. Schmidt-Ullrich, R., and Paus, R. (2005). Molecular principles of hair follicle induction and morphogenesis. BioEssays 27, 247–261. https://doi.org/10.1002/bies.20184.

6. Fuchs, E. (2007). Scratching the surface of skin development. Nature 445, 834–842. https://doi.org/10.1038/nature05659.

7. Hu, M.S., Borrelli, M.R., Hong, W.X., Malhotra, S., Cheung, A.T.M., Ransom, R.C., Rennert, R.C., Morrison, S.D., Lorenz, H.P., and Longaker, M.T. (2018). Embryonic skin development and repair. Organogenesis 14, 46–63. https://doi.org/10.1080/15476278.2017.1421882.

8. Sotiropoulou, P.A., and Blanpain, C. (2012). Development and homeostasis of the skin epidermis. Cold Spring Harb. Perspect. Biol. 4, a008383. https://doi.org/10.1101/cshperspect.a008383.

9. Mok, K.W., Saxena, N., Heitman, N., Grisanti, L., Srivastava, D., Muraro, M.J., Jacob, T., Sennett, R., Wang, Z., Su, Y., et al. (2019). Dermal condensate niche fate specification occurs prior to formation and is placode progenitor dependent. Dev. Cell 48, 32–48.e5. https://doi.org/10.1016/j.devcel.2018.11.034.

10. Gupta, K., Levinsohn, J., Linderman, G., Chen, D., Sun, T.Y., Dong, D., Taketo, M.M., Bosenberg, M., Kluger, Y., Choate, K., et al. (2019). Single-cell analysis reveals a hair follicle dermal niche molecular differentiation trajectory that begins prior to morphogenesis. Dev. Cell 48, 17–31.e6. https://doi.org/10.1016/j.devcel.2018.11.032.

11. Ge, W., Tan, S.J., Wang, S.H., Li, L., Sun, X.F., Shen, W., and Wang, X. (2020). Single-cell transcriptome profiling reveals dermal and epithelial cell fate decisions during embryonic hair follicle development. Theranostics 10, 7581–7598. https://doi.org/10.7150/thno.44306.

12. Biggs, L.C., Mäkelä, O.J.M., Myllymäki, S.M., Das Roy, R., Närhi, K., Pispa, J., Mustonen, T., and Mikkola, M.L. (2018). Hair follicle dermal condensation forms via FGF20 primed cell cycle exit, cell motility, and aggregation. eLife 7, 1–33. https://doi.org/10.7554/eLife.36468.

13. Driskell, R.R., Lichtenberger, B.M., Hoste, E., Kretzschmar, K., Simons, B.D., Charalambous, M., Ferron, S.R., Herault, Y., Pavlovic, G., Ferguson-Smith, A.C., et al. (2013). Distinct fibroblast lineages determine dermal architecture in skin development and repair. Nature 504, 277–281. https://doi.org/10.1038/nature12783.

14. Rinkevich, Y., Walmsley, G.G., Hu, M.S., Maan, Z.N., Newman, A.M., Drukker, M., Januszyk, M., Krampitz, G.W., Gurtner, G.C., Lorenz, H.P., et al. (2015). Skin fibrosis. Identification and isolation of a dermal lineage with intrinsic fibrogenic potential. Science 348, aaa2151. https://doi.org/10.1126/science.aaa2151.

15. La Manno, G., Soldatov, R., Zeisel, A., Braun, E., Hochgerner, H., Petukhov, V., Lidschreiber, K., Kastriti, M.E., Lönnerberg, P., Furlan, A., et al. (2018). RNA velocity of single cells. Nature 560, 494–498. https://doi.org/10.1038/s41586-018-0414-6.

16. Barresi, M.J.F., and Gilbert, S.F. (2020). Developmental Biology 12th Editi (Oxford University Press).

17. Yamashita, S., Miyaki, S., Kato, Y., Yokoyama, S., Sato, T., Barrionuevo, F., Akiyama, H., Scherer, G., Takada, S., and Asahara, H. (2012). L-Sox5 and Sox6 proteins enhance chondrogenic miR-140 microRNA expression by strengthening dimeric Sox9 activity. J. Biol. Chem. 287, 22206–22215. https://doi.org/10.1074/jbc.M112.343194.

18. Zuo, C., Wang, L., Kamalesh, R.M., Bowen, M.E., Moore, D.C., Dooner, M.S., Reginato, A.M., Wu, Q., Schorl, C., Song, Y., et al. (2018). SHP2 regulates skeletal cell fate by modifying SOX9 expression and transcriptional activity. Bone Res. 6, 12. https://doi.org/10.1038/s41413-018-0013-z.

19. Bartoletti, G., Dong, C., Umar, M., and He, F. (2020). Pdgfra regulates multipotent cell differentiation toward chondrocytes via inhibiting Wnt9a/beta-catenin pathway during chondrocranial cartilage development. Dev. Biol. 466, 36–46. https://doi.org/10.1016/j.ydbio.2020.08.004.

20. Bosserhoff, A.K., and Buettner, R. (2003). Establishing the protein MIA (melanoma inhibitory activity) as a marker for chondrocyte differentiation. Biomaterials 24, 3229–3234. https://doi.org/10.1016/S0142-9612(03)00184-4.

21. Chen, D., Jarrell, A., Guo, C., Lang, R., and Atit, R. (2012). Dermal beta-catenin activity in response to epidermal Wnt ligands is required for fibroblast proliferation and hair follicle initiation. Development 139, 1522–1533. https://doi.org/10.1242/dev.076463.

22. Andl, T., Reddy, S.T., Gaddapara, T., and Millar, S.E. (2002). WNT signals are required for the initiation of hair follicle development. Dev. Cell 2, 643–653. https://doi.org/10.1016/S1534-5807(02)00167-3.

23. Enshell-Seijffers, D., Lindon, C., Kashiwagi, M., and Morgan, B.A. (2010). β-catenin Activity in the Dermal Papilla Regulates Morphogenesis and Regeneration of Hair. Dev. Cell 18, 633–642. https://doi.org/10.1016/j.devcel.2010.01.016.

24. Tsai, S.Y., Sennett, R., Rezza, A., Clavel, C., Grisanti, L., Zemla, R., Najam, S., and Rendl, M. (2014). Wnt/β-catenin signaling in dermal condensates is required for hair follicle formation. Dev. Biol. 385, 179–188. https://doi.org/10.1016/j.ydbio.2013.11.023.

25. Fu, J., and Hsu, W. (2013). Epidermal Wnt controls hair follicle induction by orchestrating dynamic signaling crosstalk between the epidermis and dermis. J. Invest. Dermatol. 133, 890–898. https://doi.org/10.1038/jid.2012.407.

26. DasGupta, R., and Fuchs, E. (1999). Multiple roles for activated LEF/TCF transcription complexes during hair follicle development and differentiation. Development 126, 4557–4568.

27. Zhang, Y., Tomann, P., Andl, T., Gallant, N.M., Huelsken, J., Jerchow, B., Birchmeier, W., Paus, R., Piccolo, S., Mikkola, M.L., et al. (2009). Reciprocal requirements for EDA/EDAR/NF-κB and Wnt/β-catenin signaling pathways in hair follicle induction. Dev. Cell 17, 49–61. https://doi.org/10.1016/j.devcel.2009.05.011.

28. Song, Y., Boncompagni, A.C., Kim, S.S., Gochnauer, H.R., Zhang, Y., Loots, G.G., Wu, D., Li, Y., Xu, M., and Millar, S.E. (2018). Regional control of hairless versus hair-bearing skin by Dkk2. Cell Rep. 25, 2981–2991.e3. https://doi.org/10.1016/j.celrep.2018.11.017.

29. Galbiati, F., Volonte, D., Brown, A.M.C., Weinstein, D.E., Ben-Ze'ev, A., Pestell, R.G., and Lisanti, M.P. (2000). Caveolin-1 expression inhibits Wnt/β-catenin/Lef-1 signaling by recruting β-catenin to caveolae membrane domains. J. Biol. Chem. 275, 23368–23377. https://doi.org/10.1074/jbc.M002020200.

30. Pentinmikko, N., Iqbal, S., Mana, M., Andersson, S., Cognetta, A.B., Suciu, R.M., Roper, J., Luopajärvi, K., Markelin, E., Gopalakrishnan, S., et al. (2019). Notum produced by Paneth cells attenuates regeneration

of aged intestinal epithelium. Nature *571*, 398–402. https://doi.org/10.1038/s41586-019-1383-0.

31. Benias, P.C., Wells, R.G., Sackey-Aboagye, B., Klavan, H., Reidy, J., Buonocore, D., Miranda, M., Kornacki, S., Wayne, M., Carr-Locke, D.L., et al. (2018). Structure and distribution of an unrecognized interstitium in human tissues. Sci. Rep. *8*, 4947. https://doi.org/10.1038/s41598-018-23062-6.

32. Merrick, D., Sakers, A., Irgebay, Z., Okada, C., Calvert, C., Morley, M.P., Percec, I., and Seale, P. (2019). Identification of a mesenchymal progenitor cell hierarchy in adipose tissue. Science *364*, eaav2501. https://doi.org/10.1126/science.aav2501.

33. Eliazer, S., Muncie, J.M., Christensen, J., Sun, X., D'Urso, R.S., Weaver, V.M., and Brack, A.S. (2019). Wnt4 from the niche controls the Mechano-properties and quiescent state of muscle stem cells. Cell Stem Cell *25*, 654–665.e4. https://doi.org/10.1016/j.stem.2019.08.007.

34. Foulstone, E.J., Savage, P.B., Crown, A.L., Holly, J.M.P., and Stewart, C.E.H. (2003). Role of insulin-like growth factor binding protein-3 (IGFBP-3) in the differentiation of primary human adult skeletal myoblasts. J. Cell. Physiol. *195*, 70–79. https://doi.org/10.1002/jcp.10227.

35. Murphy, M.M., Lawson, J.A., Mathew, S.J., Hutcheson, D.A., and Kardon, G. (2011). Satellite cells, connective tissue fibroblasts and their interactions are crucial for muscle regeneration. Development *138*, 3625–3637. https://doi.org/10.1242/dev.064162.

36. Light, N., and Champion, A.E. (1984). Characterization of muscle epimysium, perimysium and endomysium collagens. Biochem. J. *219*, 1017–1026. https://doi.org/10.1042/bj2191017.

37. Kjaer, M. (2004). Role of extracellular matrix in adaptation of tendon and skeletal muscle to mechanical loading. Physiol. Rev. *84*, 649–698. https://doi.org/10.1152/physrev.00031.2003.

38. Sasse, J., von der Mark, H., Kühl, U., Dessau, W., and von der Mark, K. (1981). Origin of collagen types I, III, and V in cultures of avian skeletal muscle. Dev. Biol. *83*, 79–89. https://doi.org/10.1016/S0012-1606(81)80010-3.

39. Pace, R.A., Peat, R.A., Baker, N.L., Zamurs, L., Mörgelin, M., Irving, M., Adams, N.E., Bateman, J.F., Mowat, D., Smith, N.J.C., et al. (2008). Collagen VI glycine mutations: perturbed assembly and a spectrum of clinical severity. Ann. Neurol. *64*, 294–303. https://doi.org/10.1002/ana.21439.

40. Cescon, M., Gattazzo, F., Chen, P., and Bonaldo, P. (2015). Collagen VI at a glance. J. Cell Sci. *128*, 3525–3531. https://doi.org/10.1242/jcs.169748.

41. Purslow, P.P. (2002). The structure and functional significance of variations in the connective tissue within muscle. Comp. Biochem. Physiol. A Mol. Integr. Physiol. *133*, 947–966. https://doi.org/10.1016/S1095-6433(02)00141-1.

42. Tidball, J.G. (1991). Force transmission across muscle cell membranes. J. Biomech. *24*, 43–52. https://doi.org/10.1016/0021-9290(91)90376-X.

43. Gatchalian, C.L., Schachner, M., and Sanes, J.R. (1989). Fibroblasts that proliferate near denervated synaptic sites in skeletal muscle synthesize the adhesive molecules tenascin(J1), N-CAM, fibronectin, and a heparan sulfate proteoglycan. J. Cell Biol. *108*, 1873–1890. https://doi.org/10.1083/jcb.108.5.1873.

44. Gillies, A.R., and Lieber, R.L. (2011). Structure and function of the skeletal muscle extracellular matrix. Muscle Nerve *44*, 318–331. https://doi.org/10.1002/mus.22094.

45. Kühl, U., Öcalan, M., Timpl, R., Mayne, R., Hay, E., and von der Mark, K. (1984). Role of muscle fibroblasts in the deposition of type-IV collagen in the basal lamina of myotubes. Differentiation *28*, 164–172. https://doi.org/10.1111/j.1432-0436.1984.tb00279.x.

46. Sanderson, R.D., Fitch, J.M., Linsenmayer, T.R., and Mayne, R. (1986). Fibroblasts promote the formation of a continuous basal lamina during myogenesis in vitro. J. Cell Biol. *102*, 740–747. https://doi.org/10.1083/jcb.102.3.740.

47. Kolehmainen, M., Salopuro, T., Schwab, U.S., Kekäläinen, J., Kallio, P., Laaksonen, D.E., Pulkkinen, L., Lindi, V.I., Sivenius, K., Mager, U., et al. (2008). Weight reduction modulates expression of genes involved in extracellular matrix and cell death: the GENOBIN study. Int. J. Obes. *32*, 292–303. https://doi.org/10.1038/sj.ijo.0803718.

48. Joost, S., Annusver, K., Jacob, T., Sun, X., Dalessandri, T., Sivan, U., Sequeira, I., Sandberg, R., and Kasper, M. (2020). The molecular anatomy of mouse skin during hair growth and rest. Cell Stem Cell *26*, 441–457.e7. https://doi.org/10.1016/j.stem.2020.01.012.

49. Freytag, S.O., Paielli, D.L., and Gilbert, J.D. (1994). Ectopic expression of the CCAAT/enhancer-binding protein α promotes the adipogenic program in a variety of mouse fibroblastic cells. Genes Dev. *8*, 1654–1663. https://doi.org/10.1101/gad.8.14.1654.

50. Tontonoz, P., Hu, E., Graves, R.A., Budavari, A.I., and Spiegelman, B.M. (1994). mPPARg2: tissue-specific regulator of an adipocyte enhancer. Genes Dev. *8*, 1223–1234. https://doi.org/10.4324/9781843143215-76.

51. Benjamin, M. (2009). The fascia of the limbs and back - a review. J. Anat. *214*, 1–18. https://doi.org/10.1111/j.1469-7580.2008.01011.x.

52. Distel, R.J., Ro, H.S., Rosen, B.S., Groves, D.L., and Spiegelman, B.M. (1987). Nucleoprotein complexes that regulate gene expression in adipocyte differentiation: direct participation of c-fos. Cell *49*, 835–844. https://doi.org/10.1016/0092-8674(87)90621-0.

53. Ferrero, R., Rainer, P., and Deplancke, B. (2020). Toward a consensus view of mammalian adipocyte stem and progenitor cell heterogeneity. Trends Cell Biol. *30*, 937–950. https://doi.org/10.1016/j.tcb.2020.09.007.

54. Wojciechowicz, K., Gledhill, K., Ambler, C.A., Manning, C.B., and Jahoda, C.A.B. (2013). Development of the mouse dermal adipose layer occurs independently of subcutaneous adipose tissue and is marked by restricted early expression of FABP4. PLoS One *8*, e59811. https://doi.org/10.1371/journal.pone.0059811.

55. Seale, P., Sabourin, L.A., Girgis-Gabardo, A., Mansouri, A., Gruss, P., and Rudnicki, M.A. (2000). Pax7 is required for the specification of myogenic satellite cells. Cell *102*, 777–786. https://doi.org/10.1016/S0092-8674(00)00066-0.

56. Relaix, F., Montarras, D., Zaffran, S., Gayraud-Morel, B., Rocancourt, D., Tajbakhsh, S., Mansouri, A., Cumano, A., and Buckingham, M. (2006). Pax3 and Pax7 have distinct and overlapping functions in adult muscle progenitor cells. J. Cell Biol. *172*, 91–102. https://doi.org/10.1083/jcb.200508044.

57. Zammit, P.S. (2008). All muscle satellite cells are equal, but are some more equal than others? J. Cell Sci. *121*, 2975–2982. https://doi.org/10.1242/jcs.019661.

58. Zammit, P.S., Partridge, T.A., and Yablonka-Reuveni, Z. (2006). The skeletal muscle satellite cell: the stem cell that came in from the cold. J. Histochem. Cytochem. *54*, 1177–1191. https://doi.org/10.1369/jhc.6R6995.2006.

59. Grzelkowska-Kowalczyk, K. (2016). The importance of extracellular matrix in skeletal muscle development and function. In Composition and Function of the Extracellular Matrix in the Human Body, F. Travascio, ed. (IntechOpen).

60. Schiaffino, S., and Reggiani, C. (2011). Fiber types in Mammalian skeletal muscles. Physiol. Rev. *91*, 1447–1531. https://doi.org/10.1152/physrev.00031.2010.

61. Rubenstein, A.B., Smith, G.R., Raue, U., Begue, G., Minchev, K., Ruf-Zamojski, F., Nair, V.D., Wang, X., Zhou, L., Zaslavsky, E., et al. (2020). Single-cell transcriptional profiles in human skeletal muscle. Sci. Rep. *10*, 1–15. https://doi.org/10.1038/s41598-019-57110-6.

62. Pisconti, A., Bernet, J.D., and Olwin, B.B. (2012). Syndecans in skeletal muscle development, regeneration and homeostasis. Muscles Ligaments Tendons J. *2*, 1–9.

63. Hayward, L.J., and Schwartz, R.J. (1986). Sequential expression of chicken actin genes during myogenesis. J. Cell Biol. *102*, 1485–1493. https://doi.org/10.1083/jcb.102.4.1485.

64. Jin, S., Guerrero-Juarez, C.F., Zhang, L., Chang, I., Ramos, R., Kuan, C.H., Myung, P., Plikus, M.V., and Nie, Q. (2021). Inference and analysis of cell-cell communication using CellChat. Nat. Commun. *12*, 1088. https://doi.org/10.1038/s41467-021-21246-9.

65. Holstege, G., and Blok, B.F. (1989). Descending pathways to the cutaneus trunci muscle motoneuronal cell group in the cat. J. Neurophysiol. *62*, 1260–1269. https://doi.org/10.1152/jn.1989.62.6.1260.

66. Theriault, E., and Diamond, J. (1988). Nociceptive cutaneous stimuli evoke localized contractions in a skeletal muscle. J. Neurophysiol. *60*, 446–462. https://doi.org/10.1152/jn.1988.60.2.446.

67. Petruska, J.C., Barker, D.F., Garraway, S.M., Trainer, R., Fransen, J.W., Seidman, P.A., Soto, R.G., Mendell, L.M., and Johnson, R.D. (2014). Organization of sensory input to the nociceptive-specific cutaneous trunk muscle reflex in rat, an effective experimental system for examining nociception and plasticity. J. Comp. Neurol. *522*, 1048–1071. https://doi.org/10.1002/cne.23461.

68. Tan-Sindhunata, M.B., Mathijssen, I.B., Smit, M., Baas, F., De Vries, J.I., Van Der Voorn, J.P., Kluijt, I., Hagen, M.A., Blom, E.W., Sistermans, E., et al. (2015). Identification of a Dutch founder mutation in MUSK causing fetal akinesia deformation sequence. Eur. J. Hum. Genet. *23*, 1151–1157. https://doi.org/10.1038/ejhg.2014.273.

69. Reist, N.E., Werle, M.J., and McMahan, U.J. (1992). Agrin released by motor neurons induces the aggregation of acetylcholine receptors at neuromuscular junctions. Neuron *8*, 865–868. https://doi.org/10.1016/0896-6273(92)90200-W.

70. Joost, S., Jacob, T., Sun, X., Annusver, K., La Manno, G., Sur, I., and Kasper, M. (2018). Single-cell transcriptomics of traced epidermal and hair follicle stem cells reveals rapid adaptations during wound healing. Cell Rep. *25*, 585–597.e7. https://doi.org/10.1016/j.celrep.2018.09.059.

71. Kriehuber, E., Breiteneder-Geleff, S., Groeger, M., Soleiman, A., Schoppmann, S.F., Stingl, G., Kerjaschki, D., and Maurer, D. (2001). Isolation and characterization of dermal lymphatic and blood endothelial cells reveal stable and functionally specialized cell lineages. J. Exp. Med. *194*, 797–808. https://doi.org/10.1084/jem.194.6.797.

72. Kidoya, H., Naito, H., Muramatsu, F., Yamakawa, D., Jia, W., Ikawa, M., Sonobe, T., Tsuchimochi, H., Shirai, M., Adams, R.H., et al. (2015). APJ regulates parallel alignment of arteries and veins in the skin. Dev. Cell *33*, 247–259. https://doi.org/10.1016/j.devcel.2015.02.024.

73. Poliakov, A., Cotrina, M., and Wilkinson, D.G. (2004). Diverse roles of eph receptors and ephrins in the regulation of cell migration and tissue assembly. Dev. Cell *7*, 465–480. https://doi.org/10.1016/j.devcel.2004.09.006.

74. Wigle, J.T., and Oliver, G. (1999). Prox1 function is required for the development of the murine lymphatic system. Cell *98*, 769–778. https://doi.org/10.1016/S0092-8674(00)81511-1.

75. Ordóñez, N.G. (2012). Immunohistochemical endothelial markers: a review. Adv. Anat. Pathol. *19*, 281–295. https://doi.org/10.1097/PAP.0b013e3182691c2a.

76. Alitalo, K., Tammela, T., and Petrova, T.V. (2005). Lymphangiogenesis in development and human disease. Nature *438*, 946–953. https://doi.org/10.1038/nature04480.

77. Betterman, K.L., and Harvey, N.L. (2018). Histological and morphological characterization of developing dermal lymphatic vessels. In Lymphangiogenesis – Methods and Protocols, G. Oliver and M.L. Kahn, eds. (Springer Science+Business Media), pp. 19–35.

78. Ribatti, D., Vacca, A., and Presta, M. (2000). The discovery of angiogenic factors: A historical review. Gen. Pharmacol. *35*, 227–231. https://doi.org/10.1016/S0306-3623(01)00112-4.

79. Betsholtz, C. (2018). Cell–cell signaling in blood vessel development and function. EMBO Mol. Med. *10*, 2–5. https://doi.org/10.15252/emmm.201708610.

80. Ruhrberg, C., Gerhardt, H., Golding, M., Watson, R., Ioannidou, S., Fujisawa, H., Betsholtz, C., and Shima, D.T. (2002). Spatially restricted patterning cues provided by heparin-binding VEGF-A control blood vessel branching morphogenesis. Genes Dev. *16*, 2684–2698. https://doi.org/10.1101/gad.242002.

81. Mignatti, P., and Rifkin, D.B.B. (1996). Plasminogen activators and matrix metalloproteinases in angiogenesis. Enzyme Protein *49*, 117–137. https://doi.org/10.1159/000468621.

82. Detmar, M. (2000). The role of VEGF and thrombospondins in skin angiogenesis. J. Dermatol. Sci. *24*, S78–S84. https://doi.org/10.1016/S0923-1811(00)00145-6.

83. Luttun, A., Tjwa, M., and Carmeliet, P. (2002). Placental growth factor (PlGF) and its receptor Flt-1 (VEGFR-1). Ann. N. Y. Acad. Sci. *979*, 80–93.

84. Cao, R., Bråkenhielm, E., Li, X., Pietras, K., Widenfalk, J., Östman, A., Eriksson, U., and Cao, Y. (2002). Angiogenesis stimulated by PDGF-CC, a novel member in the PDGF family, involves activation of PDGFR-aa and -ap receptors. FASEB J. *16*, 1575–1583. https://doi.org/10.1096/fj.02-0319com.

85. David, L., Feige, J.J., and Bailly, S. (2009). Emerging role of bone morphogenetic proteins in angiogenesis. Cytokine Growth Factor Rev. *20*, 203–212. https://doi.org/10.1016/j.cytogfr.2009.05.001.

86. Goumans, M.-J., and Mummery, C. (2000). Function analysis of the TGFbeta receptor/Smad pathway through gene ablation in mice. Int. J. Dev. Biol. *44*, 253–265.

87. Newman, A.C., Nakatsu, M.N., Chou, W., Gershon, P.D., and Hughes, C.C.W. (2011). The requirement for fibroblasts in angiogenesis: fibroblast-derived matrix proteins are essential for endothelial cell lumen formation. Mol. Biol. Cell *22*, 3791–3800. https://doi.org/10.1091/mbc.E11-05-0393.

88. Shima, D.T., and Mailhos, C. (2000). Vascular developmental biology: getting nervous. Curr. Opin. Genet. Dev. *10*, 536–542. https://doi.org/10.1016/S0959-437X(00)00124-6.

89. Malhotra, R., Stenn, K.S., Fernandez, L.A., and Braverman, I.M. (1989). Angiogenic properties of normal and psoriatic skin associate with epidermis, not dermis. Lab. Invest. *61*, 162–165.

90. Soriano, P. (1994). Abnormal kidney development and hematological disorders in PDGF β- receptor mutant mice. Genes Dev. *8*, 1888–1896. https://doi.org/10.1101/gad.8.16.1888.

91. Levéen, P., Pekny, M., Gebre-Medhin, S., Swolin, B., Larsson, E., and Betsholtz, C. (1994). Mice deficient for PDGF B show renal, cardiovascular, and hematological abnormalities. Genes Dev. *8*, 1875–1887. https://doi.org/10.1101/gad.8.16.1875.

92. Gerhardt, H., and Betsholtz, C. (2003). Endothelial-pericyte interactions in angiogenesis. Cell Tissue Res. *314*, 15–23. https://doi.org/10.1007/s00441-003-0745-x.

93. Muhl, L., Genové, G., Leptidis, S., Liu, J., He, L., Mocci, G., Sun, Y., Gustafsson, S., Buyandelger, B., Chivukula, I.V., et al. (2020). Single-cell analysis uncovers fibroblast heterogeneity and criteria for fibroblast and mural cell identification and discrimination. Nat. Commun. *11*, 3953. https://doi.org/10.1038/s41467-020-17740-1.

94. Stratman, A.N., Schwindt, A.E., Malotte, K.M., and Davis, G.E. (2010). Endothelial-derived PDGF-BB and HB-EGF coordinately regulate pericyte recruitment during vasculogenic tube assembly and stabilization. Blood *116*, 4720–4730. https://doi.org/10.1182/blood-2010-05-286872.

95. Benjamin, L.E., Hemo, I., and Keshet, E. (1998). A plasticity for blood vessel remodelling is defined by pericyte coverage of the performed endothelial network and is regulated by PDGF-B and VEGF. Development *125*, 1591–1598.

96. Reynolds, L.P., Grazul-Bilska, A.T., and Redmer, D.A. (2000). Angiogenesis in the corpus luteum. Endocrine *12*, 1–9. https://doi.org/10.1385/ENDO:12:1:1.

97. Amselgruber, W.M., Schäfer, M., and Sinowatz, F. (1999). Angiogenesis in the bovine corpus luteum: an immunocytochemical and ultrastructural study. Anat. Histol. Embryol. *28*, 157–166. https://doi.org/10.1046/j.1439-0264.1999.00195.x.

98. Henri, S., Poulin, L.F., Tamoutounour, S., Ardouin, L., Guilliams, M., De Bovis, B., Devilard, E., Viret, C., Azukizawa, H., Kissenpfennig, A., et al.

(2010). CD207+ CD103+ dermal dendritic cells cross-present keratinocyte-derived antigens irrespective of the presence of Langerhans cells. J. Exp. Med. *207*, 189–206. https://doi.org/10.1084/jem.20091964.

99. Haniffa, M., Shin, A., Bigley, V., McGovern, N., Teo, P., See, P., Wasan, P.S., Wang, X.N., Malinarich, F., Malleret, B., et al. (2012). Human Tissues Contain CD141 hi Cross-Presenting dendritic Cells with Functional Homology to Mouse CD103 + nonlymphoid dendritic Cells. Immunity *37*, 60–73. https://doi.org/10.1016/j.immuni.2012.04.012.

100. Merad, M., and Manz, M.G. (2009). Dendritic cell homeostasis. Blood *113*, 3418–3427. https://doi.org/10.1182/blood-2008-12-180646.

101. Nussenzweig, M.C., Steinman, R.M., Gutchinov, B., and Cohn, Z.A. (1980). Development cells are accessory cells for the of anti-trinitrophenyl. J. Exp. Med. *152*, 1070–1084.

102. Pierre, P., Turley, S.J., Gatti, E., Hull, M., Meltzer, J., Mirza, A., Inaba, K., Steinman, R.M., and Mellman, I. (1997). Developmental regulation of invariant chain proteolysis controls MHC class II trafficking in mouse dendritic cells. Nature *388*, 787–792. https://doi.org/10.1016/S0092-8674(00)81458-0.

103. Steinman, R.M., Gutchinov, B., Witmer, M.D., and Nussenzweig, M.C. (1978). Dendritic cells are the principal stimulators of the primary mixed leukocyte reaction in mice. Proc. Natl. Acad. Sci. USA *75*, 5132–5136.

104. Förster, R., Schubel, A., Breitfeld, D., Kremmer, E., Renner-Müller, I., Wolf, E., and Lipp, M. (1999). CCR7 coordinates the primary immune response by establishing functional microenvironments in secondary lymphoid organs. Cell *99*, 23–33. https://doi.org/10.1016/S0092-8674(00)80059-8.

105. Mildner, A., and Jung, S. (2014). Development and function of dendritic cell subsets. Immunity *40*, 642–656. https://doi.org/10.1016/j.immuni.2014.04.016.

106. Tamoutounour, S., Guilliams, M., Montanana Sanchis, F., Liu, H., Terhorst, D., Malosse, C., Pollet, E., Ardouin, L., Luche, H., Sanchez, C., et al. (2013). Origins and functional specialization of macrophages and of conventional and monocyte-derived dendritic cells in mouse skin. Immunity *39*, 925–938. https://doi.org/10.1016/j.immuni.2013.10.004.

107. Hashimoto, D., Miller, J., and Merad, M. (2011). Dendritic cell and macrophage heterogeneity in vivo. Immunity *35*, 323–335. https://doi.org/10.1016/j.immuni.2011.09.007.

108. Gautier, E.L., Shay, T., Miller, J., Greter, M., Jakubzick, C., Ivanov, S., Helft, J., Chow, A., Elpek, K.G., Gordonov, S., et al. (2012). Gene-expression profiles and transcriptional regulatory pathways that underlie the identity and diversity of mouse tissue macrophages. Nat. Immunol. *13*, 1118–1128. https://doi.org/10.1038/ni.2419.

109. Hoeffel, G., Wang, Y., Greter, M., See, P., Teo, P., Malleret, B., Leboeuf, M., Low, D., Oller, G., Almeida, F., et al. (2012). Adult Langerhans cells derive predominantly from embryonic fetal liver monocytes with a minor contribution of yolk sac-derived macrophages. J. Exp. Med. *209*, 1167–1181. https://doi.org/10.1084/jem.20120340.

110. Hoeffel, G., Chen, J., Lavin, Y., Low, D., Almeida, F.F., See, P., Beaudin, A.E., Lum, J., Low, I., Forsberg, E.C., et al. (2015). C-Myb+ erythromyeloid progenitor-derived fetal monocytes give rise to adult tissue-resident macrophages. Immunity *42*, 665–678. https://doi.org/10.1016/j.immuni.2015.03.011.

111. Ginhoux, F., and Merad, M. (2010). Ontogeny and homeostasis of Langerhans cells. Immunol. Cell Biol. *88*, 387–392. https://doi.org/10.1038/icb.2010.38.

112. Chorro, L., Sarde, A., Li, M., Woollard, K.J., Chambon, P., Malissen, B., Kissenpfennig, A., Barbaroux, J.B., Groves, R., and Geissmann, F. (2009). Langerhans cell (LC) proliferation mediates neonatal development, homeostasis, and inflammation-associated expansion of the epidermal LC network. J. Exp. Med. *206*, 3089–3100. https://doi.org/10.1084/jem.20091586.

113. Dwyer, D.F., Barrett, N.A., Austen, K.F., Kim, E.Y., Brenner, M.B., Shaw, L., Yu, B., Goldrath, A., Mostafavi, S., and Regev, A. (2016). Expression profiling of constitutive mast cells reveals a unique identity within the immune system. Nat. Immunol. *17*, 878–887. https://doi.org/10.1038/ni.3445.

114. Gentek, R., Ghigo, C., Hoeffel, G., Bulle, M.J., Msallam, R., Gautier, G., Launay, P., Chen, J., Ginhoux, F., and Bajénoff, M. (2018). Hemogenic endothelial fate mapping reveals dual developmental origin of mast cells. Immunity *48*, 1160–1171.e5. https://doi.org/10.1016/j.immuni.2018.04.025.

115. Hayashi, C., Sonoda, T., Nakano, T., Nakayama, H., and Kitamura, Y. (1985). Mast-cell precursors in the skin of mouse embryos and their deficiency in embryos of sl/Sld genotype. Dev. Biol. *109*, 234–241. https://doi.org/10.1016/0012-1606(85)90363-X.

116. Kuhlbrodt, K., Herbarth, B., Sock, E., Hermans-Borgmeyer, I., and Wegner, M. (1998). Sox10, a novel transcriptional modulator in glial cells. J. Neurosci. *18*, 237–250. https://doi.org/10.1523/JNEUROSCI.18-01-00237.1998.

117. Martin, P. (1990). Tissue patterning in the developing mouse limb. Int. J. Dev. Biol. *34*, 323–336. https://doi.org/10.1387/ijdb.1702679.

118. Jenkins, B.A., and Lumpkin, E.A. (2017). Developing a sense of touch. Dev. *144*, 4048–4090. https://doi.org/10.1242/dev.120402.

119. Peng, K., Sant, D., Andersen, N., Silvera, R., Camarena, V., Piñero, G., Graham, R., Khan, A., Xu, X.M., Wang, G., et al. (2020). Magnetic separation of peripheral nerve-resident cells underscores key molecular features of human Schwann cells and fibroblasts: an immunochemical and transcriptomics approach. Sci. Rep. *10*, 18433. https://doi.org/10.1038/s41598-020-74128-3.

120. Frank, E., and Sanes, J.R. (1991). Lineage of neurons and glia in chick dorsal root ganglia: analysis in vivo with a recombinant retrovirus. Development *111*, 895–908.

121. Yamagishi, S.I., Ogasawara, S., Mizukami, H., Yajima, N., Wada, R.I., Sugawara, A., and Yagihashi, S. (2008). Correction of protein kinase C activity and macrophage migration in peripheral nerve by pioglitazone, peroxisome proliferator activated-gamma-ligand, in insulin-deficient diabetic rats. J. Neurochem. *104*, 491–499. https://doi.org/10.1111/j.1471-4159.2007.05050.x.

122. Allen, S.J., and Dawbarn, D. (2006). Clinical relevance of the neurotrophins and their receptors. Clin. Sci. (Lond) *110*, 175–191. https://doi.org/10.1042/CS20050161.

123. Roosterman, D., Goerge, T., Schneider, S.W., Bunnett, N.W., and Steinhoff, M. (2006). Neuronal control of skin function: the skin as a neuroimmunoendocrine organ. Physiol. Rev. *86*, 1309–1379. https://doi.org/10.1152/physrev.00026.2005.

124. Ansel, J.C., Kaynard, A.H., Armstrong, C.A., Olerud, J., Bunnett, N., and Payan, D. (1996). Skin-nervous system interactions. J. Invest. Dermatol. *106*, 198–204. https://doi.org/10.1111/1523-1747.ep12330326.

125. Botchkarev, V.A., Yaar, M., Peters, E.M.J., Raychaudhuri, S.K.S.P., Botchkareva, N.V., Marconi, A., Raychaudhuri, S.K.S.P., Paus, R., and Pincelli, C. (2006). Neurotrophins in skin biology and pathology. J. Investig. Dermatol. *126*, 1719–1727. https://doi.org/10.1038/sj.jid.5700270.

126. Di Marco, E., Marchisio, P.C., Bondanza, S., Franzi, A.T., Cancedda, R., and De Luca, M. (1991). Growth-regulated synthesis and secretion of biologically active nerve growth factor by human keratinocytes. J. Biol. Chem. *266*, 21718–21722. https://doi.org/10.1016/s0021-9258(18)54695-0.

127. Roggenkamp, D., Falkner, S., Stäb, F., Petersen, M., Schmelz, M., and Neufang, G. (2012). Atopic keratinocytes induce increased neurite outgrowth in a coculture model of porcine dorsal root ganglia neurons and human skin cells. J. Invest. Dermatol. *132*, 1892–1900. https://doi.org/10.1038/jid.2012.44.

128. Movafagh, S., Hobson, J.P., Spiegel, S., Kleinman, H.K., Zukowska, Z., Movafagh, S., Hobson, J.P., Spiegel, S., Kleinman, H.K., and Zukowska, Z. (2006). Neuropeptide Y induces migration, proliferation, and tube formation of endothelial cells bimodally via Y1, Y2, and Y5 receptors. FASEB J. *20*, 1924–1926. https://doi.org/10.1096/fj.05-4770fje.

129. Paus, R., Theoharides, T.C., and Arck, P.C. (2006). Neuroimmunoendocrine circuitry of the "brain-skin connection.". Trends Immunol. 27, 32–39. https://doi.org/10.1016/j.it.2005.10.002.

130. Chang, A.Y., Wanat, K.A., and Seykora, J.T. (2014). Dermatopathology. Melanocytes and vitiligo (and Hair Graying). In Pathobiology of Human Disease: A Dynamic Encyclopedia of Disease Mechanisms, L, M. McManus, ed. (Elsevier Science & Technology), pp. 1148–1157.

131. Ostrowski, S.M., and Fisher, D.E. (2018). Chapter 20. Pigmentation and melanocyte biology. In Fitzpatrick's Dermatology, S. Kang, M. Amagai, A.L. Bruckner, A.H. Enk, D.J. Margolis, A.J. McMichael, and J.S. Orringer, eds. (McGraw-Hill Education).

132. Cichorek, M., Wachulska, M., Stasiewicz, A., and Tymińska, A. (2013). Skin melanocytes: biology and development. Postepy Dermatol. Alergol. 30, 30–41. https://doi.org/10.5114/pdia.2013.33376.

133. Yoshida, H., Kunisada, T., Kusakabe, M., Nishikawa, S.S.I., and Nishikawa, S.I. (1996). Distinct stages of melanocyte differentiation revealed by analysis of nonuniform pigmentation patterns. Development 122, 1207–1214.

134. Mayer, T.C. (1973). The migratory pathway of neural crest cells into the skin of mouse embryos. Dev. Biol. 34, 39–46. https://doi.org/10.1016/0012-1606(73)90337-0.

135. Hirobe, T. (1984). Histochemical survey of the distribution of the epidermal melanoblasts and melanocytes in the mouse during fetal and postnatal periods. Anat. Rec. 208, 589–594. https://doi.org/10.1002/ar.1092080414.

136. Suzuki, I., Tada, A., Ollmann, M.M., Barsh, G.S., Im, S., Lamoreux, M.L., Hearing, V.J., Nordlund, J.J., and Abdel-Malek, Z.A. (1997). Agouti signaling protein inhibits melanogenesis and the response of human melanocytes to α-melanotropin. J. Invest. Dermatol. 108, 838–842. https://doi.org/10.1111/1523-1747.ep12292572.

137. Reddy, S., Andl, T., Bagasra, A., Lu, M.M., Epstein, D.J., Morrisey, E.E., and Millar, S.E. (2001). Characterization of Wnt gene expression in developing and postnatal hair follicles and identification of Wnt5a as a target of Sonic hedgehog in hair follicle morphogenesis. Mech. Dev. 107, 69–82. https://doi.org/10.1016/S0925-4773(01)00452-X.

138. Richardson, R.J., Hammond, N.L., Coulombe, P.A., Saloranta, C., Nousiainen, H.O., Salonen, R., Berry, A., Hanley, N., Headon, D., Karikoski, R., et al. (2014). Periderm prevents pathological epithelial adhesions during embryogenesis. J. Clin. Invest. 124, 3891–3900. https://doi.org/10.1172/JCI71946.

139. M'Boneko, V., and Merker, H.J. (1988). Development and morphology of the periderm of mouse embryos (days 9–12 of gestation). Acta Anat. (Basel) 133, 325–336.

140. Hammond, N.L., Dixon, J., and Dixon, M.J. (2019). Periderm: life-cycle and function during orofacial and epidermal development. Semin. Cell Dev. 91, 75–83. https://doi.org/10.1016/j.semcdb.2017.08.021.

141. McGowan, K.M., and Coulombe, P.A. (1998). Onset of keratin 17 expression coincides with the definition of major epithelial lineages during skin development. J. Cell Biol. 143, 469–486. https://doi.org/10.1083/jcb.143.2.469.

142. Morita, K., Furuse, M., Yoshida, Y., Itoh, M., Sasaki, H., Tsukita, S., and Miyachi, Y. (2002). Molecular architecture of tight junctions of periderm differs from that of the maculae occludentes of epidermis. J. Invest. Dermatol. 118, 1073–1079. https://doi.org/10.1046/j.1523-1747.2002.01774.x.

143. De La Garza, G., Schleiffarth, J.R., Dunnwald, M., Mankad, A., Weirather, J.L., Bonde, G., Butcher, S., Mansour, T.A., Kousa, Y.A., Fukazawa, C.F., et al. (2013). Interferon regulatory factor 6 promotes differentiation of the periderm by activating expression of grainyhead-like 3. J. Invest. Dermatol. 133, 68–77. https://doi.org/10.1038/jid.2012.269.

144. Dale, B.A., Holbrook, K.A., Kimball, J.R., Hoff, M., and Sun, T.T. (1985). Expression of epidermal keratins and filaggrin during human fetal skin development. J. Cell Biol. 101, 1257–1269. https://doi.org/10.1083/jcb.101.4.1257.

145. Morita, R., Sanzen, N., Sasaki, H., Hayashi, T., Umeda, M., Yoshimura, M., Yamamoto, T., Shibata, T., Abe, T., Kiyonari, H., et al. (2021). Tracing the origin of hair follicle stem cells. Nature 594, 547–552. https://doi.org/10.1038/s41586-021-03638-5.

146. Lechler, T., and Fuchs, E. (2005). Asymmetric cell divisions promote stratification and differentiation of mammalian skin. Nature 437, 275–280. https://doi.org/10.1038/nature03922.

147. Damen, M., Wirtz, L., Soroka, E., Khatif, H., Kukat, C., Simons, B.D., and Bazzi, H. (2021). High proliferation and delamination during skin epidermal stratification. Nat. Commun. 12, 3227. https://doi.org/10.1038/s41467-021-23386-4.

148. Cockburn, K., Annusver, K., Gonzalez, D.G., Ganesan, S., May, D.P., Mesa, K.R., Kawaguchi, K., Kasper, M., and Greco, V. (2022). Gradual differentiation uncoupled from cell cycle exit generates heterogeneity in the epidermal stem cell layer. Nat. Cell Biol. 24, 1692–1700. https://doi.org/10.1038/s41556-022-01021-8.

149. Blanpain, C., Lowry, W.E., Pasolli, H.A., and Fuchs, E. (2006). Canonical notch signaling functions as a commitment switch in the epidermal lineage. Genes Dev. 20, 3022–3035. https://doi.org/10.1101/gad.1477606.

150. Rangarajan, A., Talora, C., Okuyama, R., Nicolas, M., Mammucari, C., Oh, H., Aster, J.C., Krishna, S., Metzger, D., Chambon, P., et al. (2001). Notch signaling is a direct determinant of keratinocyte growth arrest and entry into differentiation. EMBO J. 20, 3427–3436. https://doi.org/10.1093/emboj/20.13.3427.

151. Miroshnikova, Y.A., Le, H.Q., Schneider, D., Thalheim, T., Rübsam, M., Bremicker, N., Polleux, J., Kamprad, N., Tarantola, M., Wang, I., et al. (2018). Adhesion forces and cortical tension couple cell proliferation and differentiation to drive epidermal stratification. Nat. Cell Biol. 20, 69–80. https://doi.org/10.1038/s41556-017-0005-z.

152. Lin, Z.Z., Jin, S., Chen, J., Li, Z., Lin, Z.Z., Tang, L., Nie, Q., and Andersen, B. (2020). Murine interfollicular epidermal differentiation is gradualistic with GRHL3 controlling progression from stem to transition cell states. Nat. Commun. 11, 5434. https://doi.org/10.1038/s41467-020-19234-6.

153. Rhee, H., Polak, L., and Fuchs, E. (2006). Lhx2 maintains stem cell character in hair follicles. Science 312, 1946–1949. https://doi.org/10.1126/science.1128004.

154. Levy, V., Lindon, C., Harfe, B.D., and Morgan, B.A. (2005). Distinct stem cell populations regenerate the follicle and interfollicular epidermis. Dev. Cell 9, 855–861. https://doi.org/10.1016/j.devcel.2005.11.003.

155. Ahtiainen, L., Lefebvre, S., Lindfors, P.H., Renvoisé, E., Shirokova, V., Vartiainen, M.K., Thesleff, I., and Mikkola, M.L. (2014). Directional cell migration, but not proliferation, drives hair placode morphogenesis. Dev. Cell 28, 588–602. https://doi.org/10.1016/j.devcel.2014.02.003.

156. Närhi, K., Järvinen, E., Birchmeier, W., Taketo, M.M., Mikkola, M.L., Thesleff, I., Narhi, K., Jarvinen, E., Birchmeier, W., and Taketo, M.M. (2008). Sustained epithelial b-catenin activity induces precocious hair development but disrupts hair follicle down-growth and hair shaft formation. Development 135, 1019–1028. https://doi.org/10.1242/dev.016550.

157. Fliniaux, I., Mikkola, M.L., Lefebvre, S., and Thesleff, I. (2008). Identification of dkk4 as a target of Eda-A1/Edar pathway reveals an unexpected role of ectodysplasin as inhibitor of Wnt signalling in ectodermal placodes. Dev. Biol. 320, 60–71. https://doi.org/10.1016/j.ydbio.2008.04.023.

158. Xiao, Y., Woo, W.-M., Nagao, K., Li, W., Terunuma, A., Mukouyama, Y.S., Oro, A.E., Vogel, J.C., and Brownell, I. (2013). Perivascular hair follicle stem cells associate with a venule annulus. J. Invest. Dermatol. 133, 2324–2331. https://doi.org/10.1038/jid.2013.167.

159. Brownell, I., Guevara, E., Bai, C.B., Loomis, C.A., and Joyner, A.L. (2011). Nerve-derived sonic hedgehog defines a niche for hair follicle stem cells capable of becoming epidermal stem cells. Cell Stem Cell 8, 552–565. https://doi.org/10.1016/j.stem.2011.02.021.

160. Adachi, T., Kobayashi, T., Sugihara, E., Yamada, T., Ikuta, K., Pittaluga, S., Saya, H., Amagai, M., and Nagao, K. (2015). Hair follicle–derived IL-7 and IL-15 mediate skin-resident memory T cell homeostasis and lymphoma. Nat. Med. 21, 1272–1279. https://doi.org/10.1038/nm.3962.

161. Wang, E.C.E., Dai, Z., Ferrante, A.W., Drake, C.G., and Christiano, A.M. (2019). A subset of TREM2 + dermal macrophages secretes oncostatin M to maintain hair follicle stem cell quiescence and inhibit hair growth. Cell Stem Cell *24*, 654–669.e6. https://doi.org/10.1016/j.stem.2019.01.011.

162. Sennett, R., Wang, Z., Rezza, A., Grisanti, L., Roitershtein, N., Sicchio, C., Mok, K.W., Heitman, N.J., Clavel, C., Ma'ayan, A., et al. (2015). An integrated transcriptome atlas of embryonic hair follicle progenitors, their niche, and the developing skin. Dev. Cell *34*, 577–591. https://doi.org/10.1016/j.devcel.2015.06.023.

163. Fan, X., Wang, D., Burgmaier, J.E., Teng, Y., Romano, R.A., Sinha, S., and Yi, R. (2018). Single cell and open chromatin analysis reveals molecular origin of epidermal cells of the skin. Dev. Cell *47*, 21–37.e5. https://doi.org/10.1016/j.devcel.2018.08.010.

164. Sulic, A., Roy, R. Das, Papagno, V., Lan, Q., and Saikkonen, R. (2022). Transcriptomic landscape of early hair follicle and epidermal development. https://doi.org/10.1101/2022.11.03.515012.

165. Atit, R., Sgaier, S.K., Mohamed, O.A., Taketo, M.M., Dufort, D., Joyner, A.L., Niswander, L., and Conlon, R.A. (2006). B-catenin activation is necessary and sufficient to specify the dorsal dermal fate in the mouse. Dev. Biol. *296*, 164–176. https://doi.org/10.1016/j.ydbio.2006.04.449.

166. Amini-Nik, S., Glancy, D., Boimer, C., Whetstone, H., Keller, C., and Alman, B.A. (2011). Pax7 expressing cells contribute to dermal Wound repair, regulating scar size through a β-catenin mediated process. Stem Cells *29*, 1371–1379. https://doi.org/10.1002/stem.688.

167. Lepper, C., Partridge, T.A., and Fan, C.M. (2011). An absolute requirement for pax7-positive satellite cells in acute injury-induced skeletal muscle regeneration. Development *138*, 3639–3646. https://doi.org/10.1242/dev.067595.

168. Foster, D.S., Januszyk, M., Yost, K.E., Chinta, M.S., Gulati, G.S., Nguyen, A.T., Burcham, A.R., Salhotra, A., Ransom, R.C., Henn, D., et al. (2021). Integrated spatial multiomics reveals fibroblast fate during tissue repair. Proc. Natl. Acad. Sci. USA *118*, 1–10. https://doi.org/10.1073/pnas.2110025118.

169. Phan, Q.M., Sinha, S., Biernaskie, J., and Driskell, R.R. (2021). Single-cell transcriptomic analysis of small and large wounds reveals the distinct spatial organization of regenerative fibroblasts. Exp. Dermatol. *30*, 92–101. https://doi.org/10.1111/exd.14244.

170. Guerrero-Juarez, C.F., Dedhia, P.H., Jin, S., Ruiz-Vega, R., Ma, D., Liu, Y., Yamaga, K., Shestova, O., Gay, D.L., Yang, Z., et al. (2019). Single-cell analysis reveals fibroblast heterogeneity and myeloid-derived adipocyte progenitors in murine skin wounds. Nat. Commun. *10*, 650. https://doi.org/10.1038/s41467-018-08247-x.

171. Sun, X., Annusver, K., Dalessandri, T., and Kasper, M. (2022). Rare Gli1+ perivascular fibroblasts promote skin wound repair. https://doi.org/10.1101/2022.05.16.491785.

172. Phan, Q.M., Fine, G.M., Salz, L., Herrera, G.G., Wildman, B., Driskell, I.M., and Driskell, R.R. (2020). Lef1 expression in fibroblasts maintains developmental potential in adult skin to regenerate wounds. eLife *9*, 1–19. https://doi.org/10.7554/eLife.60066.

173. Driskell, R.R., Jahoda, C.A.B.B., Chuong, C.-M.M., Watt, F.M., and Horsley, V. (2014). Defining dermal adipose tissue. Exp. Dermatol. *23*, 629–631. https://doi.org/10.1111/exd.12450.

174. Collins, C.A., Kretzschmar, K., and Watt, F.M. (2011). Reprogramming adult dermis to a neonatal state through epidermal activation of -catenin. Development *138*, 5189–5199. https://doi.org/10.1242/dev.064592.

175. Donati, G., Proserpio, V., Lichtenberger, B.M., Natsuga, K., Sinclair, R., Fujiwara, H., and Watt, F.M. (2014). Epidermal Wnt/β-catenin signaling regulates adipocyte differentiation via secretion of adipogenic factors. Proc. Natl. Acad. Sci. USA *111*, E1501–E1509. https://doi.org/10.1073/pnas.1312880111.

176. Lichtenberger, B.M., Mastrogiannaki, M., and Watt, F.M. (2016). Epidermal β-catenin activation remodels the dermis via paracrine signalling to distinct fibroblast lineages. Nat. Commun. *7*, 10537. https://doi.org/10.1038/ncomms10537.

177. Donati, G., Rognoni, E., Hiratsuka, T., Liakath-Ali, K., Hoste, E., Kar, G., Kayikci, M., Russell, R., Kretzschmar, K., Mulder, K.W., et al. (2017). Wounding induces dedifferentiation of epidermal Gata6 + cells and acquisition of stem cell properties. Nat. Cell Biol. *19*, 603–613. https://doi.org/10.1038/ncb3532.

178. Qian, H., Badaloni, A., Chiara, F., Stjernberg, J., Polisetti, N., Nihlberg, K., Consalez, G.G., and Sigvardsson, M. (2013). Molecular characterization of prospectively isolated multipotent mesenchymal progenitors provides new insight into the cellular identity of mesenchymal stem cells in mouse bone marrow. Mol. Cell. Biol. *33*, 661–677. https://doi.org/10.1128/MCB.01287-12.

179. Stuart, T., Butler, A., Hoffman, P., Hafemeister, C., Papalexi, E., Mauck, W.M., Hao, Y., Stoeckius, M., Smibert, P., and Satija, R. (2019). Comprehensive integration of single-cell data. Cell *177*, 1888–1902.e21. https://doi.org/10.1016/j.cell.2019.05.031.

180. Bergen, V., Lange, M., Peidli, S., Wolf, F.A., and Theis, F.J. (2020). Generalizing RNA velocity to transient cell states through dynamical modeling. Nat. Biotechnol. *38*, 1408–1414. https://doi.org/10.1038/s41587-020-0591-3.

181. Wolf, F.A., Angerer, P., and Theis, F.J. (2018). SCANPY: large-scale single-cell gene expression data analysis. Genome Biol. *19*, 15. https://doi.org/10.1186/s13059-017-1382-0.

182. Polański, K., Young, M.D., Miao, Z., Meyer, K.B., Teichmann, S.A., and Park, J.E. (2020). BBKNN: fast batch alignment of single cell transcriptomes. Bioinformatics *36*, 964–965. https://doi.org/10.1093/bioinformatics/btz625.

183. Lange, M., Bergen, V., Klein, M., Setty, M., Reuter, B., Bakhti, M., Lickert, H., Ansari, M., Schniering, J., Schiller, H.B., et al. (2022). CellRank for directed single-cell fate mapping. Nat. Methods *19*, 159–170. https://doi.org/10.1038/s41592-021-01346-6.

184. Schindelin, J., Arganda-Carreras, I., Frise, E., Kaynig, V., Longair, M., Pietzsch, T., Preibisch, S., Rueden, C., Saalfeld, S., Schmid, B., et al. (2012). Fiji: an open-source platform for biological-image analysis. Nat. Methods *9*, 676–682. https://doi.org/10.1038/nmeth.2019.

185. Madisen, L., Zwingman, T.A., Sunkin, S.M., Oh, S.W., Zariwala, H.A., Gu, H., Ng, L.L., Palmiter, R.D., Hawrylycz, M.J., Jones, A.R., et al. (2010). A robust and high-throughput Cre reporting and characterization system for the whole mouse brain. Nat. Neurosci. *13*, 133–140. https://doi.org/10.1038/nn.2467.

186. Andrews, T.S., and Hemberg, M. (2019). M3Drop: dropout-based feature selection for scRNASeq. Bioinformatics *35*, 2865–2867. https://doi.org/10.1093/bioinformatics/bty1044.

187. Traag, V.A., Waltman, L., and van Eck, N.J. (2019). From Louvain to Leiden: guaranteeing well-connected communities. Sci. Rep. *9*, 5233. https://doi.org/10.1038/s41598-019-41695-z.

188. Ramilowski, J.A., Goldberg, T., Harshbarger, J., Kloppmann, E., Lizio, M., Satagopam, V.P., Itoh, M., Kawaji, H., Carninci, P., Rost, B., et al. (2015). A draft network of ligand-receptor-mediated multicellular signalling in human. Nat. Commun. *6*, 7866. https://doi.org/10.1038/ncomms8866.

189. Cabello-Aguilar, S., Alame, M., Kon-Sun-Tack, F., Fau, C., Lacroix, M., and Colinge, J. (2020). SingleCellSignalR: inference of intercellular networks from single-cell transcriptomics. Nucleic Acids Res. *48*, e55. https://doi.org/10.1093/nar/gkaa183.

STAR★METHODS

KEY RESOURCES TABLE

REAGENT or RESOURCE	SOURCE	IDENTIFIER
Antibodies		
Rabbit polyclonal anti-ACTC1	Thermo Fisher Scientific	Cat# PA5-21396; RRID: AB_11152296
Rat monoclonal anti-CD45 (clone 30-F11)	Thermo Fisher Scientific	Cat# 14-0451-82; RRID: AB_467251
Rabbit polyclonal anti-KRT5	US Biological	Cat# C9097-37A2; RRID: AB_2134158
Goat polyclonal anti-GATA6	R&D Systems	Cat# AF1700; RRID: AB_2108901
Rabbit monoclonal anti-PPARG	Thermo Fisher Scientific	Cat# MA5-14889; RRID: AB_10985650
Goat polyclonal anti-PLP1	Abcam	Cat# ab61682; RRID: AB_944751
Goat polyclonal anti-PDGFRA	R&D Systems	Cat# AF1062; RRID: AB_2236897
Chemicals, Peptides, and Recombinant proteins		
DAPI	Invitrogen	Cat# D1306; RRID: AB_2629482
TO-PRO-3	Invitrogen	Cat# T3605
WGA (CF405M conjugate)	Biotium	Cat# 29028
WGA (AF488 conjugate)	Invitrogen	Cat# W11261
WGA (AF647 conjugate)	Invitrogen	Cat# W32466
HBSS	Sigma	Cat# H9394
PBS	Sigma	Cat# D8537
BSA	Sigma	Cat# A3311
Dispase II	Gibco	Cat# 17105041
DNase I	Roche	Cat# 10104159001
Collagenase IA	Sigma	Cat# C2674
Tamoxifen	Sigma	Cat# T5648
Corn Oil	Sigma	Cat# C8267
DIVA Decloaker	Biocare Medical	Cat# DV2004MX
Critical Commercial Assays		
Chromium Single Cell 3' kit v2	10X Genomics	Cat# PN-120237
RNAscope Multiplex Fluorescent Reagent Kit v2	ACDBio/Bio-Techne	Cat# 323100
TSA Cy3, Cy5, TMR, Fluorescein Evaluation Kit	PerkinElmer	Cat# NEL760001KT
Deposited Data		
Single-cell RNA-seq data	ArrayExpress	ArrayExpress: E-MTAB-11920
Input files for analysis code and critical output files (cluster assignment, UMAP coordinates, h5ad files)	Zenodo	Zenodo: https://doi.org/10.5281/zenodo.7805311
Online tool for visualization of single-cell data	Kasper Lab Website	https://kasperlab.org/embryonicskin
Experimental Models: Organisms/Strains		
Mouse: C57BL/6J	Charles River	JAX: 000664; RRID: IMSR JAX 000664
Mouse: R26-tdTomato	Jackson Laboratory	JAX: 007908; RRID: IMRS JAX 007908
Mouse: Gata6-EGFP-CreERT2	Donati et al.[177]	N/A
Mouse: Ebf2-EGFP-CreERT2	Qian et al.[178]	N/A
Oligonucleotides		
See Table S4 for all oligonucleotides used in this study.		
Software and Algorithms		
Custom scripts and computational analysis workflow	Kasper Lab GitHub / Zenodo	Github: https://github.com/kasperlab/Jacob_et_al_2023_Developmental_Cell (release v1.0; corresponds to Zenodo: https://doi.org/10.5281/zenodo.8152645)

(Continued on next page)

Continued

REAGENT or RESOURCE	SOURCE	IDENTIFIER
Cell Ranger	10X Genomics	Github: https://github.com/10XGenomics/cellranger (release v2.0.0)
Seurat	Stuart et al.[179]	Github: https://github.com/satijalab/seurat (release v3.1.1)
Velocyto	La Manno et al.[15]	Github: https://github.com/velocyto-team/velocyto.py (release v0.17.17)
scVelo	Bergen et al.[180]	Github: https://github.com/theislab/scvelo (release v0.2.1)
Scanpy	Wolf et al.[181]	Github: https://github.com/theislab/scanpy (release v1.6.0)
Bbknn	Polánski et al.[182]	Github: https://github.com/Teichlab/bbknn (release v1.3.9)
CellRank	Lange et al.[183]	Github: https://github.com/theislab/cellrank (release v1.1.0 for epidermal cells & release v.1.5.1 for fibroblasts)
CellChat	Jin et al.[64]	Github: https://github.com/sqjin/CellChat (release v1.5.0)
Fiji	Schindelin et al.[184]	https://fiji.sc

RESOURCE AVAILABILITY

Lead contact
Further information and requests for resources and data should be directed to and will be fulfilled by the lead contact Maria Kasper (maria.kasper@ki.se).

Materials availability
This study did not generate new unique reagents.

Data and code availability
Single-cell RNA-seq data have been deposited on ArrayExpress: E-MTAB-11920. The original code has been deposited on GitHub: https://github.com/kasperlab; DOI for code release at publication on Zenodo: https://doi.org/10.5281/zenodo.8152645, and input files for the analysis pipelines and the annotated and analyzed sequencing data have been deposited on Zenodo: https://doi.org/10.5281/zenodo.7805311. The raw microscopy data that support the findings of this study are available from the lead contact upon reasonable request. Any additional information required to reanalyze the data reported in this paper is available from the lead contact upon request.

EXPERIMENTAL MODEL AND STUDY PARTICIPANT DETAILS

Mouse work
The study was performed on wild-type C57BL/6J mouse embryos (mix of males and females – gender was only determined in retrospect from the sequencing data (Figure S1E)). Timed matings to obtain embryos of specific embryonic ages were set up in the evenings and the next morning was defined as E0.5. Pregnancy after timed matings was determined by comparing weight difference between the start of the mating and 10 days after. Pregnant moms were sacrificed by cervical dislocation when embryos reached the embryonic age of 12.5, 13.5, or 14.5 days, respectively, and embryos were processed for cell isolation or paraffin-embedding.

Lineage-tracing experiments were performed by crossing previously described Gata6-EGFP-CreERT2,[177] Ebf2-EGFP-CreERT2[178] and *R26-tdTomato* knock-in strains[185] (hereafter Gata6-Tom or Ebf2-Tom). Gata6-Tom mice received i.p. injection of 2mg tamoxifen (in corn oil at a concentration of 20mg/ml) at embryonic day 13.5. Uninjected mice were used as leakiness control. Tissues were sampled either 2 days after induction of lineage tracing (i.e., E15.5) or postnatally (postnatal day 5 and 35). Ebf2-Tom mice were i.p. injected with 2mg tamoxifen (in corn oil at a concentration of 20mg/ml) at E14.5 and tissues were sampled either 2 days after induction of lineage tracing or at E18.5.

FELASA recommendations for harmonized health monitoring were followed. The mice were fed *ad libitum* and handled and housed under standard conditions. All mouse work (except Gata6-lineage tracings) was performed in the animal facility of Karolinska University Hospital Huddinge in accordance with Swedish legislation and approved by the Linköping Animal Ethics Committee. Gata6-lineage tracings were performed in the animal facility of the Molecular Biotechnology Center at the University of Turin in accordance with Italian legislation and approved by the local Animal Ethics Committee and the Italian Ministry of Health.

METHOD DETAILS

Replicates

Sequencing was performed on five embryos per embryonic time point. These five embryos originated from two litters and were sampled on two different days. All 15 samples were processed and sequenced individually and can thus serve as true biological replicates (Table S2).

Each individual staining was performed on skin samples from at least 3 different embryos per embryonic age.

Tissue embedding

Whole embryos and postnatal skin tissue were formaldehyde-fixed in 4% PFA for 24h at room temperature and subsequently processed for FFPE sections (4μm thickness). When sectioning whole embryos, tissue sections were collected close to the dorsal midline.

Fluorescent *in situ* hybridization (FISH)

For independent validation and mapping of cell populations, single-molecule FISH was performed using the RNAscope Multiplex Fluorescent Detection Kit v2 according to manufacturer's instructions using TSA with Cy3, Cy5, and/or Fluorescein on FFPE sections of the embryos. The used probes are listed in the Table S4. All sections were counterstained with either WGA-405 (1:50), WGA-488 (1:50), WGA-647 (1:50), DAPI (1:500), TO-PRO3 (1:1000) or combinations of those.

Immunofluorescence (IF)

Immunofluorescence was performed either alone or after completed RNAscope staining. Combined with RNAscope, sections were washed in TBST once and then blocked and stained as in regular IF staining. For IF without RNAscope, antigen retrieval was performed using DIVA Decloaker. The following antibody concentrations were used: ACTC1 (1:500), CD45 (1:200), KRT5 (1:50), GATA6 (1:25), PPARG (1:100), PLP1 (1:1000), and RFP (endogenous tdTomato is lost during FFPE processing, 1:200). All sections were counterstained with either WGA-405nm (1:50), WGA-488nm (1:50), WGA-647nm (1:50), DAPI (1:500), TO-PRO3 (1:1000) or combinations of those.

Imaging and image analysis

Images were acquired on a Nikon microscope equipped with a Crest V3 (CrestOptics, Italy) spinning disk and a 7-line Celesta laser box (Lumencor, USA) as tiled images (5%–15% overlap) and stitched by NIS Elements software. Subsequently, all images were processed in a uniform way (maximum intensity projection, background removal with the ''subtract background'' plug-in, brightness adjustment, pseudo-colouring) using Fiji.[184]

Cell isolation

Dorsal skin of embryos (Figure S1B) was dissected with the help of fine dissection tools and dissected skins were incubated in Dispase II (2mg/ml), Collagenase IA (0.2%), and DNAse I (20U/ul) in PBS for 40 minutes at 37°C in ultra-low attachment plates (Corning Costar) on an orbital shaker. The obtained cell suspension was passed through a 40 μm cell strainer. The flow-through was spun down, and subsequently resuspended in PBS + 0.04% BSA. Samples were transported to sequencing core facility in PBS + 0.04% BSA in Eppendorf tubes that had been coated with PBS + 20% BSA overnight. Viability of the cell suspension was determined using trypan blue on an EVE automatic cell counter.

Of note, when peeling off dorsal skin tissue there were no means to technically prevent co-isolation of cells from the tissue layers underlying skin (cells from the deeper muscle layers, interstitial cells, and/or chondrocytes). Biologically, sampling the entire embryonic outer layer (skin and underlying tissue) was important as those embryonic timepoints are/were ill-defined in terms of what can be considered skin tissue.

Library preparation, sequencing and processing of sequencing data

Single-cell cDNA libraries were prepared using the 10X Genomics Chromium Single Cell 3' kit v2 according to the manufacturer's instruction. Libraries were sequenced on the HiSeq2500 system (Illumina). Raw sequencing data was processed using the 10X Genomics Cell Ranger package and the mm10 reference genome.

QUANTIFICATION AND STATISTICAL ANALYSIS

Data analysis
Analysis workflow

All downstream data analysis was performed using a mix of custom scripts and published analysis packages as described below and in Figure S1F, utilizing a mix of R packages (most importantly Seurat) as well as Python packages (most importantly Scanpy and scVelo).[179–181]

Major decisions on analytical approaches will be presented below, while we refer to the pipelines that are deposited on GitHub: https://github.com/kasperlab for any questions regarding details such as chosen parameters.

Quality control and pre-processing

Cell-filtering was performed by sample and was based on the following criteria: (a) remove cells with <200 genes/cell, (b) remove cells with low diversity index, i.e. Shannon and inverse Simpson index (this removes red blood cells, that are naturally expressing only a small variety of genes), and (c) remove cells that are simultaneously in the lowest 0.05% quantile for genes/cell (nFeature) and for reads/cell (nUMI) and that have a contribution of mitochondrial genes of <1% or >10%. By using these combinatorial criteria, it was ensured that cells would not be excluded just because they have e.g. a lower respiratory rate (i.e., low mitochondrial percentage only).

Subsequently, all 15 samples were combined into one full dataset and filtered once more on genes being expressed in at least 5 cells. Ribosomal genes (Rps and Rpl gene families), haemoglobin genes (Hba and Hbb gene families), as well as mitochondrial genes (mt gene family) were removed, as they interfered with the identification of meaningful marker genes. Log-normalization was performed using Seurat's NormalizeData function.

Determining sex of embryos

As it was very challenging to determine the sex of the embryos during sampling (due to early developmental stage and the need to process samples quickly for sequencing), litter mates were randomly chosen for sequencing and their sex was determined in retrospect from the scRNA-seq data based on the percentage of reads coming from the X chromosome and the Y chromosome (Figure S1E). This data revealed the gender identity for each of the embryos (3 females/2 males for E12.5; 1 female/4 males for E13.5; 1 female/4 males for E14.5).

Removal of cell doublets and low-quality cells

During analysis, two small groups of doublets (keratinocyte-fibroblast doublets that clustered with keratinocytes and pericyte-fibroblast doublets that clustered with fibroblasts) were encountered as well as some low-quality keratinocytes that survived global quality control (low nFeature, low nUMI, low perc.mito). Those cells were removed, and analysis was re-run without them.

Furthermore, one cluster was identified during first-level clustering which very likely corresponds to neuronal cells (sensory neurons defined by e.g. *Neurod1* and *Pou4f1* as well as sympathetic neurons defined by e.g. *Stmn2* and *Nefm*). While the signature was rather clean, the cell population originated only from a single E13.5 embryo and thus was not reproducible and most likely the result of some tissue sampling issue. Hence, the cluster was removed. Please refer to the results section, for a discussion of why neuronal transcriptomes would not be expected in this dataset.

Removing effect of confounding factors

To counteract a slight batch effect (i.e., slightly differing characteristics such as higher percentage of histone reads and pseudogene reads) linked to one of the sampling days, linear regression was performed using Seurat's ScaleData function – a rather mild measure for data integration. Regression was performed for sampling date, as well as gender, percentage of mitochondrial genes, total read counts, and cell cycle scores (S.Score and G2M.Score) as those could also potentially influence dimensionality reduction and clustering while not representing the biological variables of interest.

Prediction of cell cycle stage

Cell cycle stage was predicted using Seurat's CellCycleScoring function.

Generation of loom files

To allow for running RNA velocity analysis on spliced and unspliced mRNAs, we generated loom files using Velocyto's run10x function with default parameters and using the mm10 reference genome.

Feature selection

Feature selection was performed using the mean-dropout-method originally suggested by Andrews and Hemberg[186] in our own implementation. The 3000 genes with the highest dropout rate given their mean expression level (across non-zero counts) were chosen to be included in further analysis.

Feature selection was performed separately for the full dataset, fibroblasts, or keratinocytes, respectively, to allow for the detection of more subtle differences within fibroblasts and keratinocytes, respectively, that were hidden in the full dataset where distinct signatures of major cell types dominate the highly variable genes.

Clustering, spatial embedding, and trajectory analysis

Clustering, spatial embedding and trajectory analysis were separately adjusted for each of the three analysed groups (full dataset, fibroblasts, and keratinocytes) as they possessed very dissimilar features. The full dataset contained very distinct cell types, while fibroblasts and keratinocytes constituted a much more homogenous cell population with more gradual expression changes. Also, the biological questions that were of interest differed strongly, so different aspects had to be emphasized and analysis was adjusted accordingly.

Full dataset. Dimensionality reduction was performed in Seurat using PCA with the most highly variable genes as input after initial scaling with Seurat's NormalizeData function (a scaling factor of 10 000 was chosen as this roughly reflects the median reads/cell among the filtered cells). Subsequently, hierarchical clustering (hclust function) was performed based on PCA-reduced data. While this clustering worked well without any further need for data integration, the downstream dimensionality reduction (UMAP) still showed signs of sampling date-derived batch effects. Thus, a batch-corrected neighbourhood graph from BBKNN[182] was used to prevent batch-derived separation in UMAP space. To this aim, the regressed dataset was transferred to Python, principal components were recalculated, BBKNN was run, and dimensionality reduction was performed using Scanpy's UMAP function, which was then used to display the results of the hierarchical clustering (Figure 1B).

Fibroblasts. Fibroblast batch correction was similarly done in Scanpy using BBKNN for UMAP representation. Next, cell clustering was performed using the Leiden algorithm,[187] revealing the fibroblast subpopulations for subsequent analysis (Figure S2A). As the dermal condensate (DC) is a structure of great importance to skin development, we decided to further subcluster the DC into *FIB EarlyDC* and *FIB LateDC* using the Leiden algorithm.

Next, we imported spliced and unspliced mRNA information (from loom files) for RNA-velocity analysis using scVelo's velocity function in the stochastic mode on the highly variable genes. The predicted dynamics were then plotted on top of the pre-computed UMAP (Figure S2B).

To further analyse cellular dynamics towards the endpoints, we used CellRank (v1.5.1) pseudotime kernel. As input to the model, we calculated velocity pseudotime with identified root cells in the FIB origin populations and end cells as extreme points based on diffusion maps. Finally, we calculated absorption probabilities for each cell to become any of the identified end points.

Keratinocytes. Dimensionality reduction was performed in Seurat using PCA with the most highly variable genes as input after initial scaling. Subsequently, hierarchical clustering (hclust function) was performed based on UMAP-reduced data. The regressed keratinocyte dataset was then transferred to Python and combined with the loom-file-derived information on spliced and unspliced mRNAs.

To better understand epidermal stratification, a subset of E14.5 cells was studied, as E14.5 is the first embryonic age to capture the full differentiation trajectory. Cells from the *EPI Basal1*, *EPI Basal2*, *EPI Basal3*, *EPI Basal4*, *EPI EarlyDiff*, and *EPI LateDiff* clusters were included in the analysis. Cells related to placode, periderm, or the *EPI BasalTagln* cluster were excluded as they could potentially interfere with the differentiation trajectory. The subset was processed as described before (PCA, BBKNN, UMAP) and velocity analysis was performed, which revealed striking dominance of the cell cycle in RNA-velocity predictions (Figure S7D). Thus, cell cycle effects were regressed out in spliced and unspliced mRNA using Scanpy's regress_out function, which resulted in a striking velocity pattern reflecting epidermal stratification (Figure S7D). Finally, CellRank in combination with diffusion maps and RNA-velocity based pseudotimes was used to find macrostates and generate a refined pseudotime, to calculate lineage drivers, and to fit a GAM model for gene expression analysis.[183] The top 200 pseudotime-dependent genes were obtained and the 40 genes among them with the earliest peak in pseudotime were displayed (Figure 7K).

Using a similar approach, the differentiation trajectory within the *EPI Periderm* cluster was analysed. Periderm cells from E14.5 were identified as a terminal state and a periderm maturation trajectory could be modelled. The top 200 pseudotime-dependent genes were obtained and the 13 genes among them with the latest peak in pseudotime were displayed (Figure S7A).

Test for differential expression of genes in cell populations

Marker genes overexpressed in certain cell populations were determined using the Wilcoxon rank sum test in the Seurat implementation. Marker genes were required to be detected in at least 20% of cells in the respective population and to have a (natural) log fold change $\geq$ 0.25 compared to all other cells. Correction for multiple testing was performed using the Bonferroni method and the threshold for the FDR (false discovery rate) adjusted p-value was set to 0.05 (Table S1).

Receptor-ligand interactions

Receptor-ligand pairing was based on the approach presented by Joost et al.[70] and CellChat, respectively. In brief, for the Joost et al. approach receptors and ligands contained in the marker gene list were considered for potential receptor-ligand pairs. For each cluster pair, receptor-ligand interactions were identified by querying a receptor-ligand database. In contrast to Joost et al.[70] the curated receptor-ligand databases from Ramilowski et al.[188] and Cabello-Aguilar et al.[189] were combined to obtain an even more complete set of potential interactions. Both databases are based on human data, but we assume that the majority of registered interaction pairs are also valid for homologous genes/proteins in mice. The code was furthermore optimized for run-time and parallel computing.

To test for the enrichment of receptor-ligand pairs between two populations, the observed number of receptor-ligand pairs was compared to the number of pairs obtained from an equally sized randomly sampled pool of receptors and ligands. For each cluster pair, this simulation was repeated 10 000 times and significantly enriched interactions (p $\leq$ 0.05 for Benjamini-Hochberg-corrected p-values) were combined into Table S3. Each ligand and receptor in this table was manually annotated with reported functions and each pair was manually scored for likely involvement in the development of vessels, nerves and the immune system (Figure S5; Table S3).

Receptor-ligand interactions were identified within and between major cell populations, fibroblast subpopulations, and epidermal subpopulations (any possible combination of them with any possible signalling directionality).

As an alternative approach, CellChat was used to identify communication patterns within and between cell groups. Using CellChat's *identifyOverExpressedGenes*, *identifyOverExpressedInteractions*, *computeCommunProb*, *computeCommunProbPathway* and *aggregateNet* functions, a cell-cell communication network was inferred for cell populations present at early (E12.5) or late (E13.5 and E14.5) time points, respectively. Separate analyses were run for signaling between muscle cells and muscle-associated fibroblast populations (in late populations; Figure 5D), signaling from all cell types to vessel, immune, or neural crest-derived cells respectively (in late populations; Figures 6D), and signaling between epidermal and fibroblast populations (in early populations; Figures S6F–S6J). Circle plots were generated using CellChat's *netVisual_aggregate* or *netVisual_circle* function, while the *netAnalysis_dot* function was used to generate the dotplots of incoming and outgoing communication patterns (all detected pathways were included).